

Artifactual log-periodicity in finite size data: Relevance for earthquake aftershocks

Y. Huang^{1,2}, A. Johansen³, M. W. Lee³, H. Saleur¹, and D. Sornette^{3,4,5}

Abstract. The recently proposed discrete scale invariance and its associated log-periodicity are an elaboration of the concept of scale invariance in which the system is scale invariant only under powers of specific values of the magnification factor. We report on the discovery of a novel mechanism for such log-periodicity relying solely on the manipulation of data. This “synthetic” scenario for log-periodicity relies on two steps: (1) the fact that approximately logarithmic sampling in time corresponds to uniform sampling in the logarithm of time; and (2) a low-pass-filtering step, as occurs in constructing cumulative functions, in maximum likelihood estimations, and in de-trending, reddens the noise and, in a finite sample, creates a maximum in the spectrum leading to a most probable frequency in the logarithm of time. We explore in detail this mechanism and present extensive numerical simulations. We use this insight to analyze the 27 best aftershock sequences studied by *Kisslinger and Jones* [1991] to search for traces of genuine log-periodic corrections to Omori’s law, which states that the earthquake rate decays approximately as the inverse of the time since the last main shock. The observed log-periodicity is shown to almost entirely result from the “synthetic scenario” owing to the data analysis. From a statistical point of view, resolving the issue of the possible existence of log-periodicity in aftershocks will be very difficult as Omori’s law describes a point process with a uniform sampling in the logarithm of the time. By construction, strong log-periodic fluctuations are thus created by this logarithmic sampling.

1. Introduction

Log-periodic corrections to scaling have been one of the most exciting topics in the physics of rupture in recent years [*Saleur and Sornette*, 1996; *Saleur et al.*, 1996a, b]. If present, these corrections might make the prediction of major events a less hopeless task [*Ani-*

frani et al., 1995] than previously thought [*Geller et al.*, 1997]. Log-periodicity is a characteristic behavior of systems exhibiting discrete scale invariance (DSI) [*Sornette*, 1998], either geometrical or spontaneously generated by the dynamics. Like all symmetries, DSI could provide a powerful new concept in the study of cracks, rupture, and disordered systems in general.

DSI is an elaboration of the concept of scale invariance, which has been broadly applied in the geosciences [*Scholz and Mandelbrot*, 1989; *Barton and Pointe*, 1995; *Turcotte*, 1997; *Sornette*, 2000]. The word “fractal” was coined by B.B. Mandelbrot to describe sets which consist of parts similar to the whole and which can be described by a fractional dimension. This generalization of the notion of a dimension from integers to real numbers reflects the conceptual jump from translation in-

¹Department of Physics, University of Southern California, Los Angeles.

²Department of Earth Sciences, University of Southern California, Los Angeles.

³Institute of Geophysics and Planetary Physics, University of California, Los Angeles.

⁴Department of Earth and Space Sciences, University of California, Los Angeles.

⁵Laboratoire de Physique de la Matière Condensée, CNRS UMR 6622 and Université de Nice-Sophia Antipolis, Nice, France.

variance to continuous scale invariance. More recently, the generalization of the notion of dimension, according to which the dimensions or exponents are taken from the set of complex numbers, has been shown to describe the interesting and rich phenomenology of systems exhibiting discrete scale invariance, associated with log-periodic corrections to scaling [Saleur and Sornette, 1996; Saleur et al., 1996a, b; Sornette, 1998]. Discrete scale invariance is a weaker kind of scale invariance in which the system or the observable obeys scale invariance only for specific choices of magnifications, which form, in general, a countably infinite set of values, all powers of a fundamental scale factor λ . This property can also be seen to include the concept of lacunarity of the fractal structure.

Log-periodic oscillations have been reported in acoustic emissions prior to rupture [Anifrani et al., 1995; Sahimi and Arbabi, 1996; Johansen and Sornette, 1998; Sornette, 1999], to rock bursts in deep mines [Ouilleton and Sornette, 2000], in precursory seismic activity before large earthquakes [Sornette and Sammis, 1995], and in anomalous ionic concentration prior to the Kobe earthquake [Johansen et al., 1996, 2000a]. The status of log-periodicity is the clearest for rupture of heterogeneous materials for which a sub-harmonic cascade of Mullins-Sekerka instabilities has been recognized as the probable underlying mechanism [Sornette et al., 1996; Huang et al., 1997]. The application to earthquakes is controversial [Gross and Rundle, 1998] as only a few case studies have been reported. In this context, a major difficulty consists of the selection of the appropriate space-time window to construct time-to-failure functions [Bowman et al., 1998; Brehm and Braile, 1999]. Another problem stems from the scarcity of seismic data relevant to this problem since only large (and thus rare) earthquakes exhibit precursory seismic activity observable solely on relatively large foreshocks [Reasenber, 1999]. Notwithstanding these limitations, further investigation of the possible existence of log-periodicity is important for its potential use (1) in constraining the mechanisms controlling earthquake triggering, (2) in focusing possible forecasting skills based on the measured accelerated seismicity, and (3) in providing indirect measurements of the stress drop ratio and the seismic efficiency [Lee, 1999].

It is fair to say, however, that the existence of log-periodic corrections in rupture is not proven beyond doubt: They have typically been observed in systems with very noisy data, and so far, we are still lacking a nontrivial analytically solvable model where they could be shown to exist rigorously. By nontrivial, we mean

a realistic model of rupture without preexisting hierarchy which could be treated analytically to prove log-periodicity. In that respect, the situation is not unlike critical phenomena, where the possibility of power law singularities was hotly debated before Onsager [1944]’s solution of the Ising model. This must be contrasted with the preexisting hierarchical geometry, such as the hierarchical diamond lattices or tent-like hierarchies or Cantor sets used by Newman et al. [1995] and Saleur and Sornette [1996]; Saleur et al. [1996a, b] for which the log-periodicity derives rather trivially by measuring the fractal dimensions of the underlying geometrical object [Sornette, 1998].

It is therefore of vital importance to have a greater understanding of the relation between apparent log-periodic corrections and noise. After the initial period of enthusiasm, the suspicion has grown, in particular, that the consideration of cumulative quantities, like the Benioff strain in foreshock sequences, might well introduce spurious log-periodicity in the data, despite the lack of any physical DSI. The purpose of this paper is to examine several scenarios where apparent log-periodic corrections are generated by the interplay of noise and the method of data analysis. We report on a basic artifactual source generating log-periodicity, which is a combination of a sampling that is periodic in a log timescale and some type of low-pass filtering such as in constructing cumulative functions, maximum likelihood estimators, and de-trending.

In the analysis of power law data, sampling is more often regular (sometimes even periodic) on a log scale than might be initially expected. For instance, in our previous analysis of the Kobe earthquake the chemical concentrations reported by Tsunogai and Wakita [1995, 1996] were sampled in a nonuniform way because the measurements were performed **after** the earthquake. Specifically, the chemical composition of groundwater prior to the earthquake was analyzed by collecting bottles of mineral water from wells close to the epicenter for which the production dates could be identified. Since the depletion process of bottles in stores can be approximated by a Poisson process with some rate μ , this implies that the number of bottles with a production date t prior to the date of the earthquake t_c is proportional to $\exp[-\mu(t_c - t)]$, quantifying an accelerated sampling in the time $t_c - t$ to the earthquake. This is not exactly a sampling that is uniform in the variable $\ln(t_c - t)$; it will nevertheless be approximately so in finite time intervals and, as a consequence, may lead to the effects discussed in this paper.

Another example occurs naturally when analyzing

aftershocks. Omori’s law for aftershocks [Utsu *et al.*, 1995] states that the rate $Q(t)$ of earthquakes following a main earthquake decays as t^{-p} , where t is the time from the main shock and p is close to 1:

$$Q(t) \propto 1/t^p. \quad (1)$$

It is equivalent to having the probability of an aftershock in the time interval $[t, t+dt]$ proportional to dt/t^p . Alternatively, the occurrence time t for an aftershock is a random variable with a power law probability distribution. When analyzing a given empirical aftershock time series, the problem of measuring the rate precisely becomes crucial. To compute the rate, one has to choose a binning interval. A constant interval is not satisfactory since Omori’s power law implies that events cluster densely at the beginning of the time series and become very sparse at long times. A binning interval varying with time is the most natural, but it will, when optimally chosen, realize once again a periodic sampling in log scale. We will discuss this in great detail in Section 3.

The spurious log-periodicity generated by such sampling will usually become amplified when considering cumulative quantities, which act as a low-pass filter. This is quite unfortunate, since taking cumulative quantities is a very natural procedure in many cases. For instance, taking the cumulative of the empirical rate of aftershocks appears to be a natural well-defined approach, which has the advantage of being nonparametric and amounts simply to counting the number of events up to a running time t .

The paper is organized as follows. In Section 2 we analyze in detail the effect of cumulating quantities on log-periodicity. In Section 2.1.3 we show that when the binning of a power law is logarithmic in time, the cumulative distribution creates splendid and totally spurious log-periodicity. Section 2.2 applies this insight to real aftershock sequences: Using this cumulative method, we find that it is not possible to distinguish any real log-periodicity from the synthetic mechanism in the 27 best aftershock sequences studied by *Kisslinger and Jones* [1991] and in the Loma Prieta, Landers, and Northridge aftershock sequences. Section 2.3 shows that, conversely, cumulating can destroy a preexisting log-periodicity, when the binning is performed regularly and nonlogarithmically. Section 3 turns to another analyzing method using maximum likelihood. We again show that the synthetic mechanism for log-periodicity operating in the cumulative method is present here, and we quantitatively demonstrate its main properties. Applied to this set of aftershock sequences, we find that

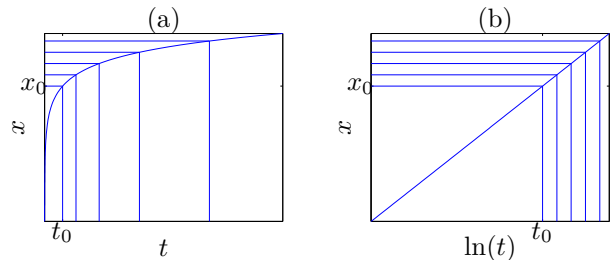


Figure 1. Mapping between a uniformly distributed random variable x and a random variable t with power law distribution: (a) linear scale for t and (b) log scale for t .

most of the observed log-periodic signal can be explained by the synthetic mechanism. However, there seems to remain a residual signature, possibly stemming from a physically based log-periodicity, which can not be accounted for by the synthetic mechanism. This evidence is not sufficiently strong to conclude definitively with high statistical significance. Section 4 summarizes our findings.

2. Cumulative Distributions and Their Fluctuations

Omori’s law (1) and, more generally, any continuous law can be obtained from a one-to-one mapping to a uniformly distributed random variable x (without loss of generality, we take $x \in [0, 1]$ when not specified otherwise):

$$x = \int_0^t Q(t') dt', \quad (2)$$

which is the cumulative distribution function (cdf) obtained from the condition of “conservation of probability” $P(x)dx = Q(t)dt$ under a change of variable. Consider the special case $p = 1$. This leads to

$$P(x)dx \sim dx \sim \frac{1}{t} dt \sim d \ln t, \quad (3)$$

which highlights the mapping between the linear scale in x and the logarithmic scale in t .

The mapping (2) is shown graphically in Figure 1. A given value x_0 on the x axis corresponds to a point t_0 on the t axis, through the transformation (2) represented by the continuous curve in Figure 1a. If x_0 is a random variable uniformly distributed on the x axis, t_0 will be a random variable with a power law distribution. A sequence of equally spaced x is mapped onto a sequence of t with increasing separation following a power law $p(t)$. Note that we are not sampling a power law function,

rather the power law probability density function (pdf) results from the spacing between the times t of the aftershocks. When t is plotted on a log scale (Figure 1b), we see that if there is a cluster of points near x_0 , there will be a cluster of points near t_0 . When the clustering of points in x is periodic on the x axis, the clustering is periodic on the $\ln t$ axis; thus periodicity in the cdf of x is mapped to log-periodicity in the cdf of t .

2.1. Theory

2.1.1. Shot-noise spectrum for cumulative distributions of finite data sets. To understand the effect of constructing cumulative quantities, we consider the cdf for the variable x uniformly distributed in $[0, u]$. The cdf is by definition $\text{cdf}(x) = x/u$ defined for $0 \leq x \leq u$. Here we add the interval size variable u to investigate how the fluctuations, in particular the most probable ones, may depend on the size of the sampled interval. Let us assume that a finite number N of values x are sampled in the interval $[0, u]$, and let us construct the empirical cdf $\text{cdf}_e(x)$ from this data set by simply counting the number of values less or equal to x and normalizing by N . We expect to get an approximate straight line with step-like fluctuations around it. These ‘‘shot noise’’ fluctuations are described by

$$\text{cdf}_e(x) = \frac{1}{N} \sum_{i=1}^N H(x - x_i), \quad (4)$$

where the Heaviside function: $H(y) = 0$ for $y < 0$ and is 1 otherwise. To study the fluctuations around the theoretical $\text{cdf}(x) = x/u$, we estimate the Fourier transform of the residual $R \equiv \text{cdf}_e(x) - x/u$, which reads

$$R = -\frac{1}{i\omega} \left[\frac{1}{N} \sum_{i=1}^N e^{i\omega x_i} - \frac{e^{i\omega u} - 1}{i\omega u} \right]. \quad (5)$$

The first term on the right-hand side gives the usual fluctuation spectrum $|R|^2 = N^{-1}\omega^{-2}$ of ‘‘red noise.’’ The other term in the r.h.s. is only present for *finite* interval size u . In the presence of a finite u , the spectrum $|R|^2$ presents correction factors with amplitude proportional to $(e^{i\omega u} - 1)/i\omega u$ and its modulus squared. These corrections describe the possible existence of oscillations with angular frequency ω decorating the linear dependence. This shows us that the finite size u of the interval introduced a nonzero most probable angular frequency. Here, by most probable, we mean the frequency corresponding to the largest peak of the spectrum. It is

defined as the angular frequency that maximizes

$$\left| \frac{e^{i\omega u} - 1}{i\omega u} \right|^2 = \frac{2}{\omega^2} [1 - \cos(\omega u)], \quad (6)$$

which is the solution of

$$\tan(\omega u/2) = \omega u/2. \quad (7)$$

Thus we find $\omega u/2 \approx 3\pi/2$. Since $\omega = 2\pi f$, this gives the most probable frequency

$$f \approx 1.5/u, \quad (8)$$

which is inversely proportional to the length u of the interval. This constitutes our first prediction.

From the structure of (5), we see that the amplitude of the leading correction to asymptotic spectrum $N^{-1}\omega^{-2}$ is proportional to $1/N$; that is, we expect the most probable oscillation decorating the linear cdf x/u to have a typical amplitude proportional to $1/\sqrt{N}$. This constitutes our second prediction.

2.1.2. Spectrum of cumulative variables that are solution of a stochastic ordinary differential equations. To show the generality of these results, we can generalize the problem within the framework of stochastic ordinary differential equations and study the ‘‘cumulative’’ variable X defined by

$$dX/du = aX + \eta(u), \quad (9)$$

where η is a white noise defined by $\langle \eta(u)\eta(u') \rangle = \delta(u - u')$, where the angle brackets mean that an ensemble average is taken. Eq. (9) allows for a deviation from the simple linear cumulative law by introducing a first-order autoregressive correlation (the aX term). The solution of (9) is

$$X(u) = \int_0^u \eta(\tau) \exp[a(u - \tau)] d\tau. \quad (10)$$

Eq. (10) shows that X is the cumulative of η , weighted by the exponential term $\exp[a(u - \tau)]$ (equal to 1 for $a = 0$). The white noise can be written as

$$\eta(\tau) = \int d\omega e^{i\omega\tau} \hat{\eta}(\omega), \quad (11)$$

which defines $\hat{\eta}(\omega)$. The stochastic variable is characterized by the following covariance: $\langle \hat{\eta}(\omega)\hat{\eta}^*(\omega') \rangle = \delta(\omega - \omega')$, where the asterisk denotes the complex conjugate. Putting (11) into (10), we get

$$X(u) = \int d\omega f_u(\omega) e^{i\phi(\omega)}, \quad (12)$$

where

$$f_u(\omega) = \frac{e^{i\omega u} - e^{au}}{i\omega - a}. \quad (13)$$

The most probable angular frequency is again obtained by maximizing $|f_u(\omega)|^2$. Let us take the limit of small a for which the noise dominates (in the power law mapping, this corresponds to an exponent p close to 1). Then (13) simplifies into

$$f_u(\omega) \approx \frac{e^{iu\omega} - 1}{i\omega} \quad (14)$$

$$|f_u(\omega)|^2 = (2/\omega^2)[1 - \cos(\omega u)]. \quad (15)$$

This retrieves the same solution (8) as above for the shot noise problem. Note that the $1/\omega^2$ spectrum for a signal with an infinite range is modified by the cosine correction observed for a finite range.

These simple calculations can be explained intuitively as follows. Consider an uncorrelated Gaussian noise. In the frequency domain the spectrum of Gaussian noise is flat (white), since all frequency components are equally probable. Let us call $G(\omega)$ the white spectrum of the measurement error $g(x)$. $G(\omega)$ does not, however, extend to all frequencies and is bounded by the measurement range of x . The lowest angular frequency ω_{\min} is determined by the span of x , corresponding to one half cycle covering the whole interval (Nyquist frequency). The highest angular frequency is determined by the distance between successive x_i .

When noise is integrated, as occurs in constructing a cumulative distribution, the resulting noise is smoother and its spectrum is reddened with more power in the low-frequency band. This results from the fact that the spectrum of $\int^x g(x')dx'$ is $\omega^{-2} G(\omega)$ [Stratonovich, 1967].

Regardless of the precise shape of $G(\omega)$ (we allow here for departure from white noise), the combination of the lower angular frequency cutoff and the ω^{-2} increase implies that $\omega^{-2}G(\omega)$ presents a well-defined peak near ω_{\min} . The left side of the peak is determined by the nature of the frequency cutoff, while the right side is controlled by the ω^{-2} decay resulting from the integration. This angular frequency peak corresponds to the most probable oscillation in the signal, *i.e.*, the frequency at which the spectrum is maximum. In other words, the integration of the white noise in finite time series creates a low-frequency periodic oscillation decorating the average trend of $\int^x g(x')dx'$.

We thus obtain the following general result: for approximately uniformly distributed random variables

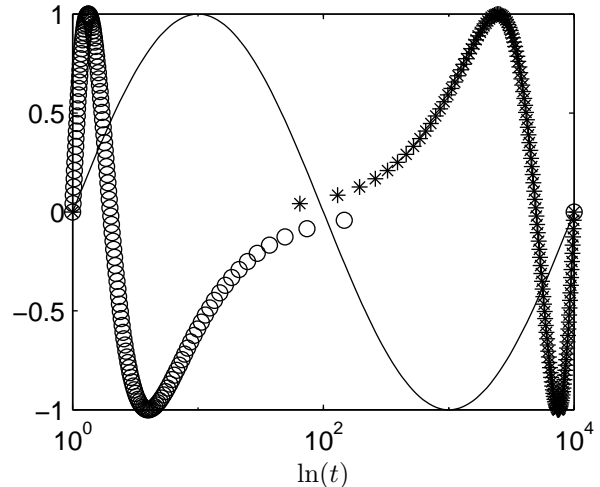


Figure 2. Mapping of a periodic function in x under the transformation (2) for $p = 1$ (solid line), $p = 2$ (circles), and $p = 0.01$ (stars).

and finite samples, the most probable oscillation decorating the cumulative distribution is inversely proportional to the range u of the variables. In addition, the amplitudes of the oscillations decay on average as the square root of the sample size. This is therefore a finite size effect.

Slutzky [1937] similarly found that taking sums **and** differences of discrete time series, *i.e.*, filtering-smoothing them, introduces oscillations in otherwise completely noisy data. See also Zajdenweber [1976] for simulations with an application to economy.

2.1.3. Application to log-periodicity in cumulative power law distributions. With the change of variable $u \rightarrow \ln t$ obtained in (3), for $p = 1$, (9) describes a power law $X \sim t^a$ decorated by noise. The previous calculations in the linear variable u translates directly to the variable $\ln t$, predicting a most probable log-periodic component with log frequency $1.5/\ln(t_2/t_1)$, where $[t_1, t_2]$ defines the interval in the variable t .

When the power exponent p is not exactly 1, the mapping curve in Figure 1b will not be a straight line, and then the mapping of a periodic function in x under the transformation (2) will not yield an exact periodic function, as shown in Figure 2.

In Figure 2 when the power law exponent p is 1 (solid line), the function is periodic in $\ln t$. For $p = 2$ (circles) the function is not exactly periodic in $\ln t$. Owing to the rapid decay of $1/t^2$, the events cluster closer to $t = 0$

than for the $1/t$ decay. In contrast, for $p < 1$ the events cluster at larger t more than for the $1/t$ decay, which leads to the oscillations shown by the stars in Figure 2 for $p = 0.01$. For more reasonable values closer to 1, we observe significant regular oscillations which are approximately log-periodic. Their significance is assessed by the existence of a significant peak in the spectrum. The approximate log frequency peak will be higher in the case of $p \neq 1$ than in the case for $p = 1$, but the difference is not very strong for the empirically relevant cases for which the apparent exponent does not deviate very much from 1. In the case of aftershocks, Omori's law is typically characterized by exponents in the range $[0.5, 2.0]$ [Kisslinger and Jones, 1991]. Similarly, the accelerating Benioff strain of precursory earthquake activity prior to a main shock is typically characterized by a power law $(t_c - t)^{-p}$ with an exponent p close to 0.5 [Bowman et al., 1998].

Therefore the generation of log-periodicity in the case of logarithmically sampled power laws relies on the following ingredients: (1) noise and sampling fluctuations (shot noise) provide all kinds of frequency components; (2) integration filters out high-frequency components, enhances low-frequency components, and produces a ω^{-2} spectrum only perturbed for the lowest frequencies for the finite range in $\ln t$ of the data set; and (3) there is a direct mapping from periodicity to log-periodicity for power laws with exponents close to $p = 1$ since data points are close to being uniformly distributed in $\ln t$ scale.

Summarizing, we expect to observe log-periodic oscillations from the integration of noise in power laws: (1) the (log-)frequencies of the log-periodic oscillations should have a power spectrum given by ω^{-2} ; (2) the most probable frequency should scale as the inverse of the range in log scale of the analysis; (3) the most probable frequency should increase when the power law exponent p deviate from 1; and (4) the amplitude of the oscillations should scale as the inverse square root of the number of data points (central limit theorem).

In Section 2.2 we present numerical tests of these predictions performed on synthetically generated samples.

2.2. Numerical Simulations

Our numerical simulations are based on the hypothesis that the noise is uncorrelated. Empirical realizations of the noise in real data sets may be of a different nature. However, we believe that our results hold by and large as our mechanism relies mainly on the existence of an increasing power spectrum at low log frequencies bounded from below by finite size effects.

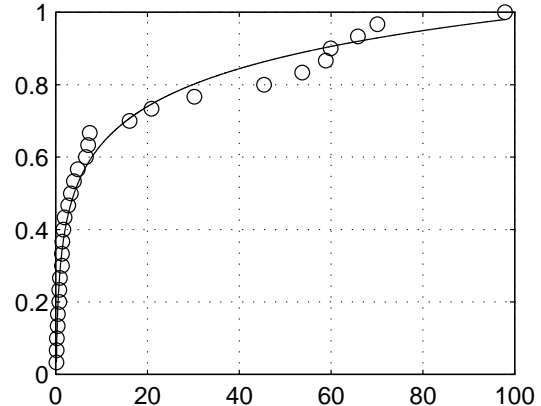


Figure 3. Circles represent the cumulative distribution of a realization of synthetic aftershocks with Omori's law ($p = 1$) obtained with (16). The solid line is a fit to the synthetic data using a power law. The vertical axis is the normalized cumulative number of events. The horizontal axis is time t (the same unit as the real sequence).

A sequence of event occurrence times t_i for $i = 1, \dots, N$ are generated within the fixed time interval $[t_0, t_u]$, with a power law rate $1/t^p$ by the transformation method [Press et al., 1992]. In this method, one starts from a uniformly distributed random variable $x \in [0, 1]$ and generates the corresponding random variables t using the transformation (2), *i.e.*,

$$t = \left[t_0^{1-p} + x \left(t_u^{1-p} - t_0^{1-p} \right) \right]^{\frac{1}{1-p}}, \quad (16)$$

on each of the realizations of the x variable. In this procedure we specify the number N of points x in $[0, 1]$, generate them in this interval using a random number generator, and apply the transformation (16) to each of these values to obtain the sequence t_i for $i = 1, \dots, N$. The cumulative distribution of a typical realization (circles) is shown in Figure 3.

In our analysis, we first determine the best power law fit to the synthetic data of Figure 3 and study its residue, shown in Figure 4. We then perform a spectral analysis of the residue to test for the presence of possible periodic oscillations. Since the data points are not evenly spaced in the $\ln t$ scale, we use the Lomb method [Press et al., 1992]. Recall that for unevenly sampled data the Lomb method is superior to fast Fourier transform (FFT) methods because it weights data on a “per

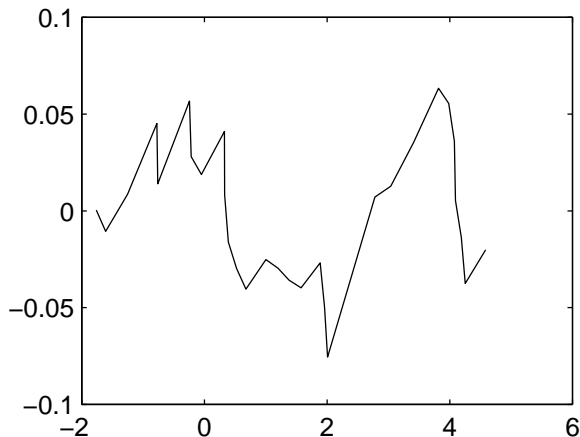


Figure 4. Oscillations around the power law (solid line) of the normalized cumulative number of events (circles) in Figure 3. The horizontal axis is $\ln t$.

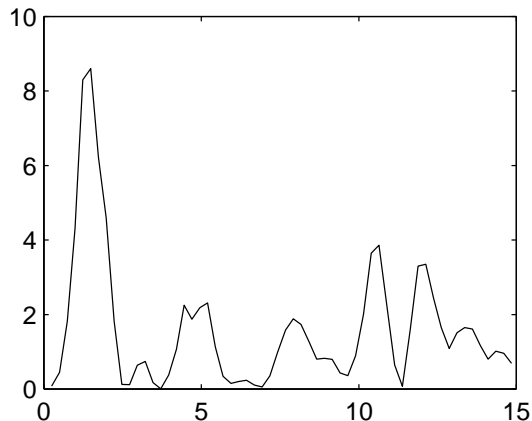


Figure 5. The spectrum of the residue shown in Figure 4. The horizontal axis is frequency ω . The vertical axis is the normalized Lomb spectral power.

point” basis instead of a “per time interval” basis. Furthermore, the significance level of any frequency component can be estimated quite accurately [Press *et al.*, 1992].

In order to determine the presence or absence of a periodic signal in the residue, it is necessary to quantify the statistical significance of the peaks found in the spectrum $P_N(\omega)$. We use the null hypothesis that the noise realizations at distinct times are uncorrelated Gaussian distributed, which in the Lomb method leads

to $P_N(\omega)$ with an exponential probability distribution with unit mean. Thus, if we scan M independent frequencies, the probability that none has a spectral peak larger than z is $(1 - e^{-z})^M$. The false alarm probability of the null hypothesis is then

$$P(\text{peak} > z) \equiv 1 - (1 - e^{-z})^M. \quad (17)$$

A small value for the false alarm level indicates a highly significant periodic signal. In general, M depends on the number of frequencies sampled, the number of data points, and their detailed spacing. Usually, M is of the order of a few N , the number of data points (for example in the Interactive Data Language (IDL) implementation of the Lomb method, $M = N$). Figure 5 shows the spectrum of the residue presented in Figure 4. One observes a main peak near $\omega = 1.5$, with height (with normalized spectral density) around 8.5. Since the number of data points here is $N = 31$, using the standard choice $M = N = 31$ gives the false alarm level 0.006 for this peak, indicating that the probability that this peak results from chance is 0.6%, which corresponds to a confidence level better than 99%.

In the following, we will consider only the most significant peak of our synthetic samples. We first run 1000 simulations with $N = 100$ data points with $t_0 = 0.1$ and $t_u = 100$. Using the estimation of the false alarm probability (17), we find that 99.4% among the 1000 synthetic time series have a significance level better than 99% for the presence of a periodic component. The distribution of these angular frequencies is shown in Figure 6 and is compatible with the theoretical prediction $\sim \omega^{-2}$ given by (15).

We now test the prediction (8) that the most probable angular frequency is inversely proportional to the range $\ln(t_{\max}/t_{\min})$ in $\ln t$ of the data set. In our tests, we set $t_{\min} = 1$ and sweep t_{\max} . For each value of t_{\max} we construct 100 runs to get the average angular frequency. Since the angular frequencies are distributed according to a power law (approximately ω^{-2}), the average is not the most probable value. However, both quantities have very similar distributions, and there is a simple proportionality relation between the average and the most probable value. We analyze the average angular frequency for computational simplicity. Figure 7 shows the average angular frequency as a linear function of $1/[\ln(t_{\max}/t_{\min})]$.

As seen in Figure 2, when the power law exponent p is not equal to 1, the mapping between periodicity in the x and log-periodicity in the t variable is not exact: the clustering of data points either at small t ($p > 1$) or at large t ($p < 1$) effectively shortens the logarithm

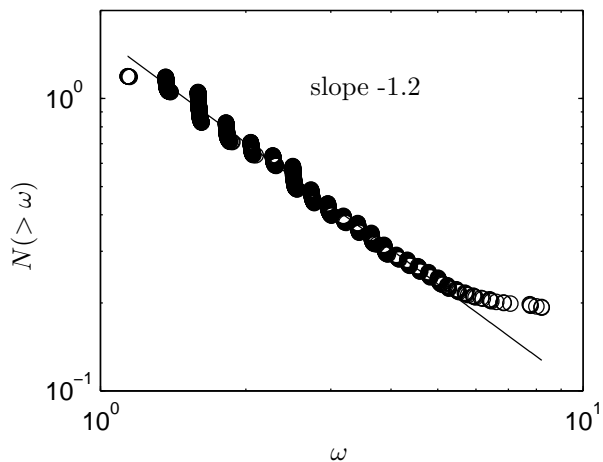


Figure 6. The cumulative distribution of the most significant angular frequencies of the log-periodic oscillations obtained from the cumulative power law distribution. The straight line is the theoretical prediction of ω^{-2} (corresponding to slope -1 in the cumulative distribution) and is included to guide the eye.

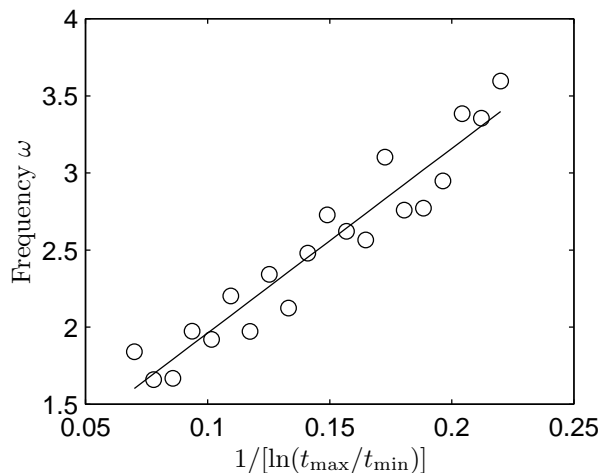


Figure 7. The average angular frequency as a function of $1/[\ln(t_{\max}/t_{\min})]$.

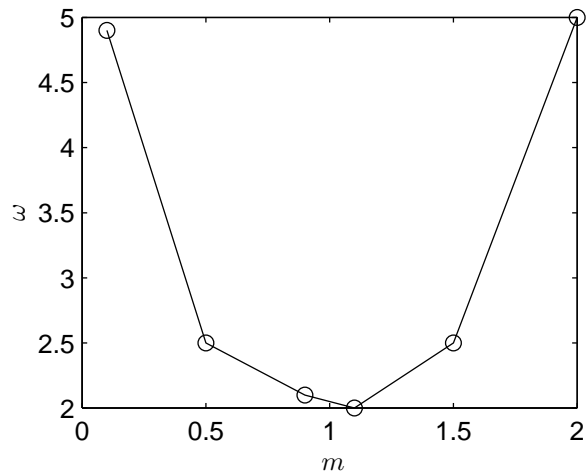


Figure 8. The most probable angular frequency ω as a function of the power law exponent m .

mic range and thus increases the effective value of the most probable frequency. We verify this prediction by generating, for each value of p , 20 runs that allow us to get an estimation of the log frequency distribution from which the most probable log angular frequency is extracted. We verify in Figure 8 that the most probable log angular frequency increases as p departs from 1.

We now test the prediction that the amplitude of the log-periodic oscillation should be proportional to $N^{-1/2}$, where N is the number of data points. For each value of N the amplitude is averaged over 20 runs. Figure 9 shows the dependence of the log-periodic oscillation amplitude for N going from 100 to 5995, with the best fit $\sim N^{-0.49}$ in excellent agreement with the prediction.

Although log-periodic oscillations from integration of noise tend to be low log frequency, corresponding to one to two oscillation cycles, our simulations show that the probability of observing oscillations that span up to 2.5 periods is still around 10%.

2.3. Tests on Real Aftershock Data

Recent numerical simulations and a mean-field analysis have been performed on models of earthquake aftershocks in one-, two-, and three-dimensional Euclidean lattices, using both continuous elasticity and discrete cellular automata modeling [Lee, 1999; Lee and Sornette, 2000]. Owing to the interplay of power law stress corrosion and the threshold nature of rupture, the average stress is found to decay in a punctuated

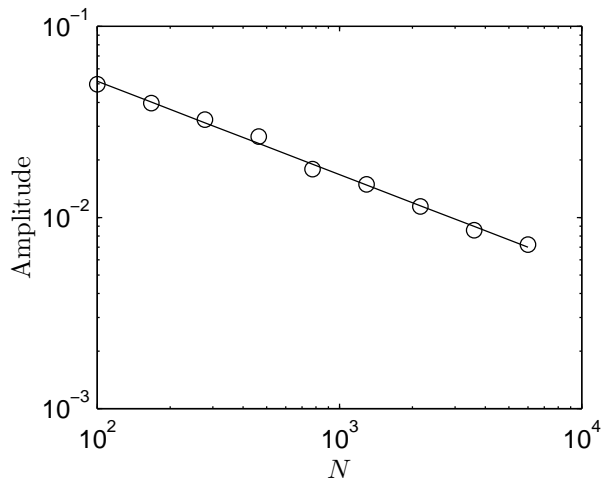


Figure 9. The scaling relation between the amplitudes of the log-periodic oscillations and the number of data points N . The slope is -0.49 .

fashion after a main shock, with events occurring at characteristic times increasing as a geometrical series with a well-defined multiplicative factor (a signature of log-periodicity) which is a function of the stress corrosion exponent, the stress drop ratio, and the degree of dissipation. These results, found independent of the discrete nature of the lattice, raise the possibility that log-periodic structures may also be observable in real aftershock data [Lee, 1999]. If confirmed, their existence would provide constraints on their underlying mechanism as well as on the stress corrosion exponent, the stress drop ratio, and the degree of dissipation. Another possible mechanism comes from the hierarchical structure of the fracturation of the crust with the coexistence of an approximate self-similarity together with characteristic scales associated with the thicknesses of geological and rheological layers [Ouilleton *et al.*, 1995, 1996]. These considerations have motivated us to search for log-periodic oscillations around Omori’s power law of the normalized cumulative number of events for 27 aftershock sequences in southern California, 1933-1988. The log-periodic components in the oscillations are extracted using the Lomb method and compared with those from synthetic aftershock sequences generated with the same parameters as the real aftershock sequences.

In order to avoid possible bias in the selection of the aftershock time series we decided to study a sufficiently large and high-quality data set that has been studied previously by an independent team, namely, the 39 af-

tershock sequences in southern California covering the time from 1933 to 1988, compiled by *Kisslinger and Jones* [1991] using the *Reasenbergy* [1985] algorithm. In addition, we studied more recent large aftershock time series from the Loma Prieta earthquake (October 1989 in northern California), the Landers earthquake (June 1992), and the Northridge earthquake (January 1994).

Kisslinger and Jones [1991] used these sequences to study the properties of aftershocks in southern California, focusing on Omori’s power law $1/t^p$ and possible correlation between the exponent p and geophysical properties like surface heat flow. They found that the temporal behavior of aftershocks is generally well-described by the modified Omori’s law. The p values range from 0.69 to 1.809, with mean value of 1.109 and standard deviation 0.246. Among the sequences, six values were graded “poor,” 10 “fair,” and 24 “good,” on the basis of the relative size of the standard error to the p value itself with a standard error $< 0.1 p$ being good, $> 0.2 p$ being poor, and fair being in between. The number of aftershocks in one sequence ranges from 12 to 1437, and the duration of the sequences ranges from 7 days to around 1000 days. Note that the sizes of the samples are adjusted by the chosen magnitude cutoffs which have been varied to test the robustness of our results.

In order to test for the possible existence of log-periodic oscillations decorating Omori’s power law we need the $1/t^p$ power law to be a good approximation in the first place. We thus discarded the poor data sets (4, 7, 8, 26, 34, 35) as defined by *Kisslinger and Jones* [1991]. We then examined the other sequences very carefully before using them, and some more sequences were discarded for some obvious reasons:

1. A sequence is severely incomplete in the early stage as seen from the plot of the temporal distribution of the events (4, 7, etc., confirming *Kisslinger and Jones’* fits).

2. There is a sudden change of properties in the middle of the sequence due to some large aftershocks which probably caused their own aftershocks (19, 21, 37, 38). This is explicitly illustrated for the two sequences 19 and 37 (for sequence 19, $p = 5.8 \pm 9.0$ from a fitting program in a commercial software system Matlab using the Levenberg-Marquardt algorithm, while *Kisslinger and Jones’* result is $p = 1.113 \pm 0.415$. For other sequences, our results are close to their results. For sequence 37, there are two subsequences with very different p , one is close to 1.1, the other is close to 2.0 according to *Kisslinger and Jones* [1991]). If the sequence is sufficiently long, we truncate it and keep the part before the

distortion for the analysis. Otherwise, we discard it.

3. The number of events is too small (say < 15) or the duration is too short (say < 1 day), for example, events 16 and 18 last 0.21 days, events 13 and 39 last 15 days.

Of the 39 aftershock sequences studied by *Kisslinger and Jones* [1991], 12 were thus excluded from our analysis. For the other 27 sequences we first change the magnitude cutoff above which the aftershocks are kept in the analysis. This allows us to determine the best magnitude cutoff for which the oscillations decorating Omori's power law for the normalized cumulative number of events are the most regular. This selection introduces a slight bias in favor of the presence of log-periodicity, which in fact strengthens our negative conclusion obtained by this approach. In any case, similar results are obtained by choosing the magnitude threshold used by *Kisslinger and Jones* [1991]. The regularity and strength of the oscillations are quantified by the ratio between the sum of the squares of the errors (RSSE) in the time domain resulting from the power law fit and from a power law with log-periodic oscillations added on it. The presence of log-periodic oscillations is also quantified by the significance level of the main peak of the oscillation spectrum obtained from the Lomb method.

We illustrate this procedure on the 1933 Long Beach earthquake sequence, with a main shock magnitude of 6.3, which contains 571 events with minimum magnitude 2.0 and total duration of 2576 days. For this sequence, using a magnitude cutoff of 4.5 provides the strongest signal: we find the smallest correction for the origin of time of the aftershock sequence (a fit to the modified Omori's law $1/(t + C)^p$ gives a very small C , an exponent p close to 1 and a high RSSE). The Lomb periodogram of the oscillations has also a very significant frequency peak. The cumulative number of events is shown in Figure 10, in which the solid line is the fit to a pure power law. The residual of this fit is shown in Figure 11 and is fitted to a simple cosine function. The corresponding spectral analysis is shown in Figure 12.

Synthetic tests were performed for this magnitude cutoff of 4.5 by generating 200 numerical sequences with exactly the same parameters as determined by the simple power law fit. Figure 13 shows that the real sequence (defined as the intersection of the two lines) exhibits a log-periodic frequency essentially equal to the most probable log frequency of the synthetic data, with a Lomb peak not so uncommon either (corresponding approximately to a 10% significance level).

Aftershock sequence 30 of the Santa Barbara Island earthquake is found to exhibit the strongest log-periodic

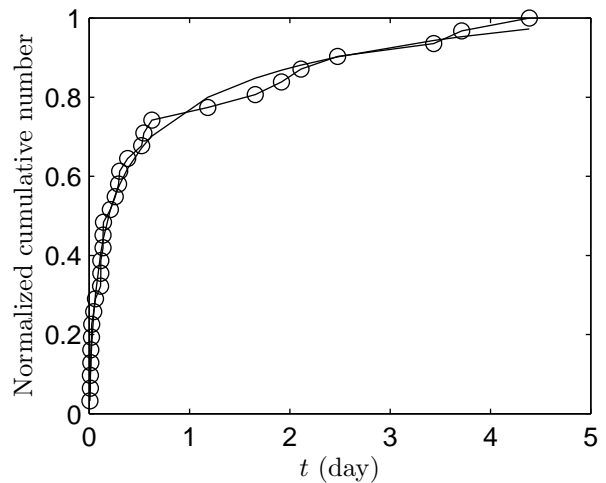


Figure 10. Cumulative number of events at the optimal magnitude cutoff 4.5 for the 1933 Long Beach earthquake aftershock sequence. The empirical data are represented by circles connected by lines to guide the eye.

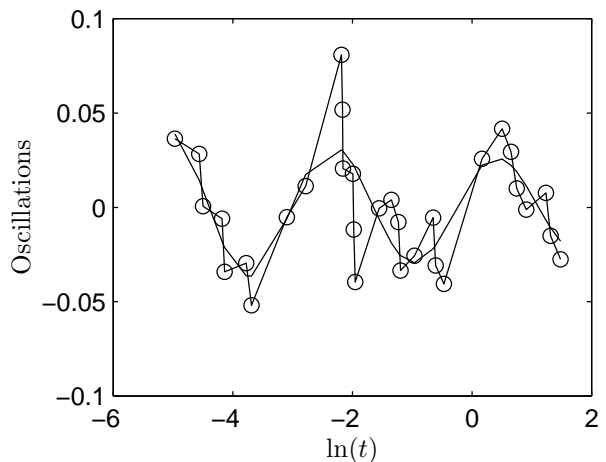


Figure 11. Residual oscillations of the fit of Figure 10 by a simple power law are themselves fitted by a simple cosine function (solid line). The empirical data are represented by circles connected by lines to guide the eye.

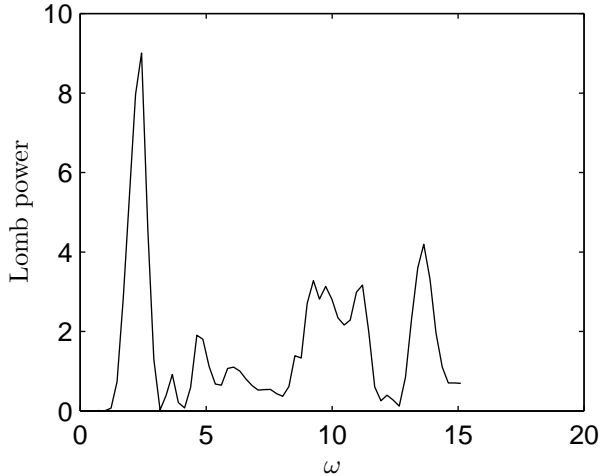


Figure 12. Spectral analysis of the oscillations shown in Figure 11 using the Lomb Periodogram for unevenly sampled data.

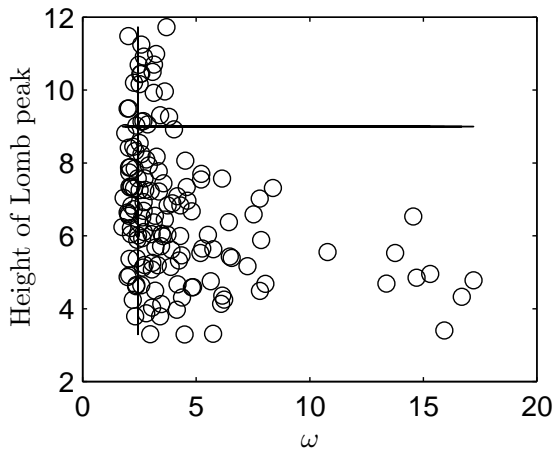


Figure 13. Distribution of the log angular frequency ω and peak height of 200 synthetic data sets and comparison to the real sequence identified as the intersection of the two lines.

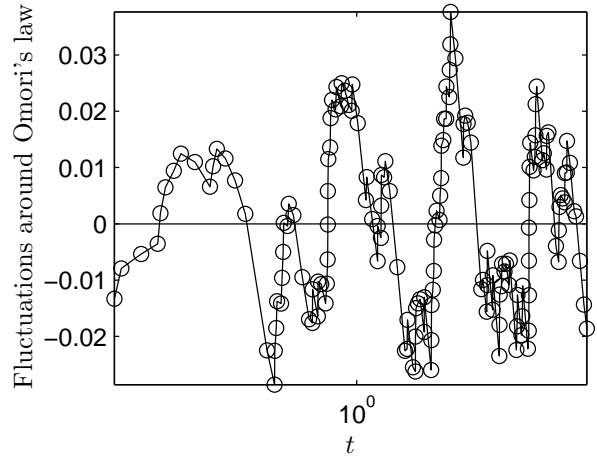


Figure 14. Log-periodic oscillations around the cumulative number of events of the Santa Barbara Island aftershock sequence 30.

oscillations, shown in Figure 14 and 15. However, from 10 synthetic sequences using the parameters from the real sequence, we observed four better log-periodic oscillations at similar log frequencies. We also find that the amplitude of oscillations of the real sequence is close to that of the synthetic sequences, and this is a general property found for all the other sequences. From more extensive simulations with 200 synthetic sequences we confirm that these oscillations shown in Figure 14 are near the most probable region of the distribution of the log frequencies in the synthetic time series.

To summarize these results, let us first discuss the time series obtained by using the magnitude cutoffs chosen by *Kisslinger and Jones* [1991]. We find that only 10 sequences among the 27 analyzed sequences have log frequencies outside the most probable range of synthetic log frequencies. Among them, seven (sequence 11, 13, 20, 22, 28, 29, 30) have log frequencies slightly higher than the most probable synthetic frequencies and might thus be considered as potential candidates for a genuine physical origin. The three other cases have log frequencies that are lower than found for most of the synthetic tests, a signature of a trend or large-scale aliasing. With respect to the statistical significance of the peaks obtained from the Lomb periodogram, only six sequences (10, 18, 23, 27, 31, 36) have spectral peaks higher than the most probable synthetic peak heights, and none of them overlap with the seven candidates selected above.

For time series constructed with the best magnitude cutoff we find that eight of the log frequencies are higher

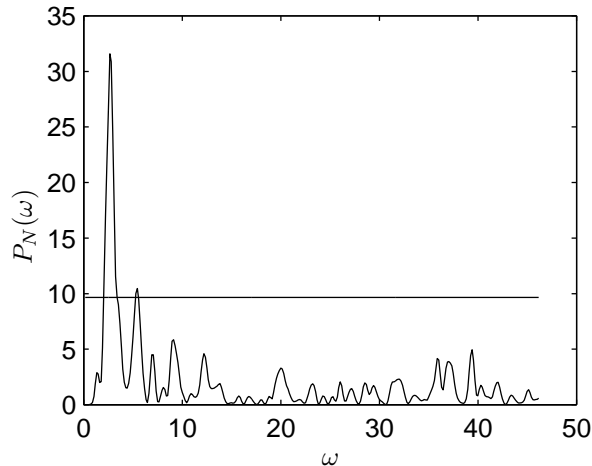


Figure 15. Normalized Lomb periodogram of the oscillations in Figure 14. The horizontal line marks significance level of 0.01.

than those found at the magnitude cutoffs of *Kisslinger and Jones* [1991], nine are lower, and ten are equal. However, the log frequencies from the corresponding synthetic data sets are also shifted accordingly. Five sequences (5, 11, 15, 23, 30) have log frequencies higher than the most probable range of the frequencies from the synthetic data sets, six sequences (1, 13, 14, 22, 27, 36) have peak higher than those from synthetic data sets, but there is no overlap between these two sets of five and six sequences, respectively. No significant improvement was thus gained by optimizing the magnitude cutoffs for more regular log-periodic oscillations. These results are summarized in Tables 1 and 2. When our choice of the best magnitude cutoff is the same as that of Kisslinger and Jones, the sequence is excluded from Table 2 to avoid repetition.

We thus find that the 27 aftershock sequences in southern California analyzed by the cumulative distribution method exhibit clear log-periodic structures, which are, however, not strongly statistically significantly different from those generated in synthetic time series. Indeed, synthetic series generated using the pure Omori’s power law exhibit similar structures that result from the noise reddening mechanism explained in sections 2.1 and 2.2. Optimization over magnitude cutoff for more regular oscillations does not significantly improve the results. We observed that log-periodic oscillations with angular log frequencies are found in the interval $[0.8, 6.2]$ in most sequences with various regularity. When compared with synthetic aftershock se-

quences, these frequencies and the power spectrum at these frequencies are found among the most probable values in synthetic sequences with the same parameters and analyzed in the same way. The amplitudes of the oscillations in the real sequences are almost equal to those of the synthetic data.

Another natural quantity to investigate in order to qualify Omori’s law (1) is to take the numerical derivative of the cumulative number \mathcal{N} of aftershocks with respect to the variable $\ln t$. For a pure Omori’s law with exponent $p = 1$, this log derivative should be constant. Any deviations from a constant provides a measure of deviation from Omori’s law. We estimate the logarithmic derivative by

$$\left. \frac{d\mathcal{N}}{d \ln(t)} \right|_{t=t_i} = \frac{\mathcal{N}(t_{i+1}) - \ln \mathcal{N}(t_{i-1})}{\ln(t_{i+1}) - \ln(t_{i-1})}. \quad (18)$$

Owing to the intermittent nature of the data, a moving average has been applied to the derivative. An example of the result is shown in Figure 16. Rather than a constant that would qualify Omori’s law, we observe quite strong approximately log-periodic signatures. However, a test on a synthetic data sequence, using the same number of points and time window as well as the same Omori’s p estimated by *Kisslinger and Jones* [1991], gives a similar signal, as shown in Figure 17, namely approximately equidistant peaks of fluctuations. The log-periodic signatures are generated from the noise and are probably not genuine. In fact, the most obvious difference between the true data and the synthetic data is that the oscillations in the synthetic data have been shifted down to shorter timescales. This is presumably due to an imprecise estimation of the value of the exponent p .

2.4. Cumulating and Log-Periodicity

The essential property of the logarithmic sampling is a flat noise spectrum (in the log variable) before integration. Integration then leads to the appearance of a low-frequency peak, as discussed in Section 2. Different samplings will give rise to different noise spectra, which, when convoluted with the integration, might well not create spurious log-periodicity, or even destroy an existing one. We now give an example of the latter situation.

We have generated 10 data sets with 30 points each using

$$y(t) = t^{-0.5} [1 + 0.1 \cos(7 \ln t)], \quad (19)$$

where the sampling was random in the sense that the spacing between two consecutive points was cho-

Table 1. Log-Periodic Signals in the Oscillations Around the Modified Omori's Power Law of the Cumulative Number of Aftershocks Using Kisslinger and Jones' Magnitude Cutoff

seq # ^a	mm ^b	ω_0^c	ω_1^d	ω^e	pkht ₀ ^f	pkht ₁ ^g	pkht ^h	Pr(Chance) ⁱ
01	6.3	1.0740	2.7077	1.7175	14.4865	35.6532	14	0.63
02	5.1	1.4913	4.2834	2.1367	1.6963	6.9105	5	0.1974
03	6	1.8340	2.5803	2.4112	4.0659	7.8017	5.5	0.4300
05	6.9	2.2869	2.8769	1.8280	3.7103	8.1253	8	0.1548
06	5.9	0.7297	1.7442	0.8516	8.0163	17.4935	9	0.8495
09	6.2	1.1510	1.4220	1.2025	22.4059	29.2246	28	0.3152
10	5.5	1.5570	2.6391	1.6537	9.7964	22.9913	37	0.005
11	6	0.8838	1.8858	2.3547	13.0106	25.0258	16	0.0606
12	5.9	1.2057	2.9265	1.5851	11.9195	26.1618	18	0.6
13	5.7	1.2308	1.7628	2.1031	3.4584	7.6336	5.8	0.2479
14	7.7	1.1584	1.3052	1.1763	31.2361	58.8183	44	0.4724
15	6.2	0.8841	2.1099	2.0406	9.4233	22.2794	16	0.0414
17	5.6	1.6172	2.4806	0.9766	1.4954	3.7202	3.7	0.28
18	6.5	0.9946	2.3998	0.9688	11.3033	18.0648	26	0.0118
20	6.6	0.6763	1.6025	2.0684	19.4909	46.3860	25	0.0863
22	5.1	1.1030	2.2221	3.6476	38.4192	47.8631	37	0.0125
23	5.8	1.1490	2.6941	1.4775	9.1692	17.2860	18	0.1907
24	5	1.1602	2.2417	1.2623	13.9662	28.9842	17	0.7714
25	5.2	1.6197	2.9343	1.9517	31.0554	50.2901	42	0.3984
27	5.5	1.0248	2.3511	1.1171	4.7256	15.4207	16	0.0914
28	6.1	1.9769	5.0416	6.2079	2.6342	9.3955	8	0.0102
29	5.7	2.1068	3.3735	3.4648	6.8699	18.2430	14	0.0278
30	5.3	1.1045	2.2538	2.6459	22.4250	45.6508	32	0.0408
31	6.5	0.7557	1.8494	1.1278	39.3589	68.9044	75	0.0811
32	5.8	1.1349	2.5303	1.8404	31.0060	53.6768	36	0.3254
33	5.9	1.2886	2.3381	1.7686	157.7374	430.4343	400	0.0950
36	6	1.0569	2.0341	1.4477	25.5461	51.6242	62	0.0308

^aThe number of the data sets used by *Kisslinger and Jones* [1991].

^bMain shock magnitude.

^cThe left-wise angular frequency at half the maximum of the distribution of angular frequencies from synthetic aftershocks.

^dThe right-wise angular frequency at half the maximum of the distribution of angular frequencies from synthetic aftershocks.

^eFrom the real aftershock sequence.

^fThe left-wise angular frequency at half the maximum of the distribution of the peak heights of the most significant Lomb peak from synthetic aftershocks.

^gThe right-wise angular frequency at half the maximum of the distribution of the peak heights of the most significant Lomb peak from synthetic aftershocks.

^hPeak height of the Lomb periodogram for the real aftershock sequence.

ⁱProbability of the log-periodicity in real aftershocks being chance.

Table 2. Log-Periodic Signals in the Oscillations Around the Modified Omori's Power Law of the Cumulative Number of Aftershocks Using Other Magnitude Cutoff^a

seq #	ω_0	ω_1	ω	pkht ₀	pkht ₁	pkht	Pr(Chance)
01	1.7518	3.6436	2.4358	3.3245	8.6912	9	0.1181
03	1.0438	3.3507	1.9949	6.0207	12.8901	11	0.0417
05	1.0686	2.8314	11.9837	4.5386	10.1490	8	0.0068
11	1.0552	2.3074	2.3547	9.5031	17.9494	16	0.0606
13	1.2473	2.8182	2.1031	3.3596	10.3787	11	0.0213
14	1.0120	2.1585	1.04	10.1416	22.0273	28	0.0357
15	0.9610	2.0448	2.2577	12.5354	34.1214	30	0.0132
17	1.1423	3.4385	1.0949	1.3481	6.9516	6	0.375
18	1.0009	2.5511	2.5486	15.9492	34.7236	30	0.0301
20	0.7923	1.8448	1.3063	52.6478	118.4051	95	0.1019
22	1.7097	3.0411	1.0599	50.9766	71.1400	95	0.005
23	1.4364	2.4938	2.6761	19.0478	56.8038	40	0.0455
24	1.3325	2.6773	1.2826	7.5998	17.1631	15	0.3005
25	1.6782	3.6164	1.7050	49.2585	71.3087	10	0.005
27	0.9257	2.2607	1.0769	7.9868	22.5240	24	0.0655
28	1.7700	3.8280	2.4337	42.6775	78.4212	12	0.005
29	1.8001	3.1963	2.4748	12.6694	26.2655	25	0.1224
30	0.9557	2.4180	2.6459	16.8089	33.8548	31	0.0408
32	1.1580	2.7235	1.6682	13.4569	33.1647	22	0.3408
33	0.9972	2.8735	2.2487	3.4352	9.3050	9	0.0588

^aMeanings as in Table 1.^aMeanings as in Table 1.

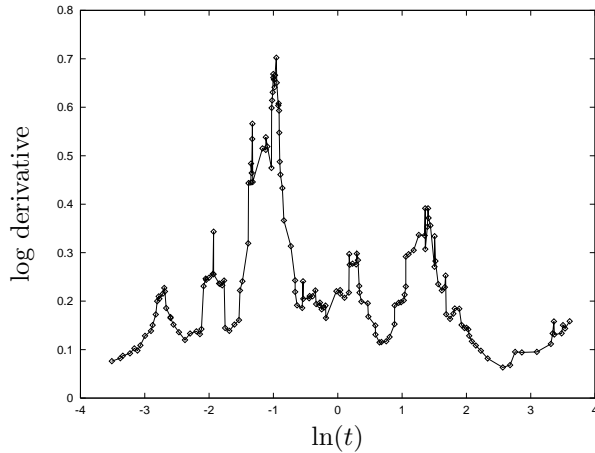


Figure 16. Aftershock sequence following the Owens Valley $M5.8$ earthquake on October 14, 1978. Derivative (denoted “log derivative”) of the cumulative number of aftershocks with respect to the logarithm of time as a function of $\ln(t)$ is shown.

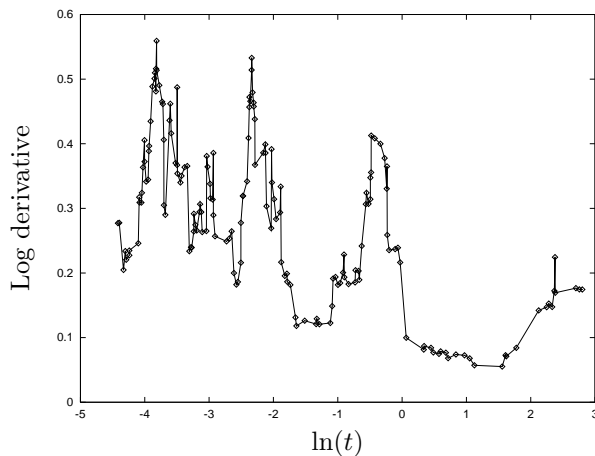


Figure 17. Same as Figure 16 for a synthetic data set corresponding to the aftershock sequence shown in Figure 16. The same number of points and time interval as in Figure 16 were used. The p value was $p \approx 1.249$ as listed by *Kisslinger and Jones* [1991].

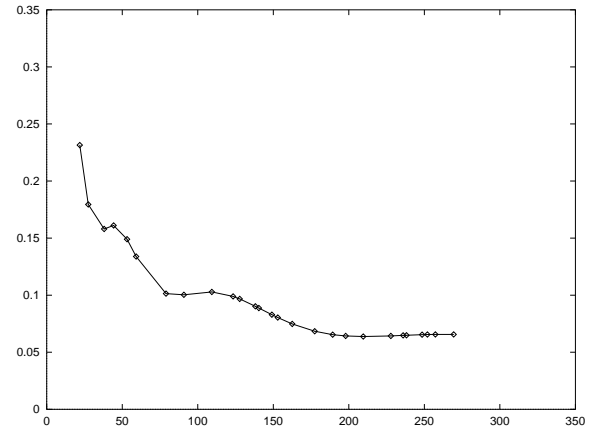


Figure 18. Typical artificial data set of 30 points generated with Eq. (19) with a random sampling such that the spacing between two consecutive points was chosen from the interval $[0, 20]$ with a uniform probability.

sen from the interval $[0, 20]$ with uniform probability. From the Lomb periodogram of the log derivative $[\ln y(t_{i+1}) - \ln y(t_i)] / [\ln t_{i+1} - \ln t_i]$ shown in Figure 19, we can clearly identify the log-periodic component in the signal and its log frequency $f = 7/2\pi \approx 1.1$ with a level of significance better than 0.995 (see Figure 22).

In contrast, the log-periodic signal completely disappears in the cumulative distribution as seen in Figure 23. This not only shows that a strong log-periodic signal will be destroyed by “integration” but also that without noise, only two to three oscillations are needed to qualify log-periodicity.

It is well-known that an integration of sampled data corresponds to a low-pass filter. What we have seen here is that this low-pass filtering extends into the log frequency domain with surprising efficiency.

3. Maximum Likelihood Analysis of the Aftershock Sequences

The previous analyses illustrate the danger of apparently innocuous manipulations of the data, such as calculating cumulative distributions of aftershock sequences. This suggests that a method that gives direct access to the local Omori’s exponent may be better suited for the unbiased detection of log-periodic structures. Indeed, the most direct quantification of departure from Omori’s law is to look at the logarithmic derivative of the total number N of events until time

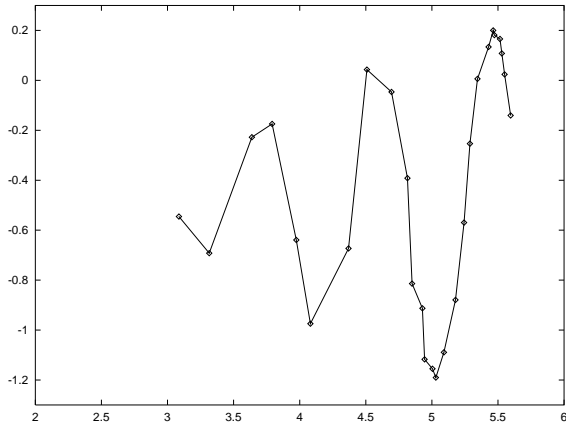


Figure 19. The logarithmic derivative of the data set in Figure 18.

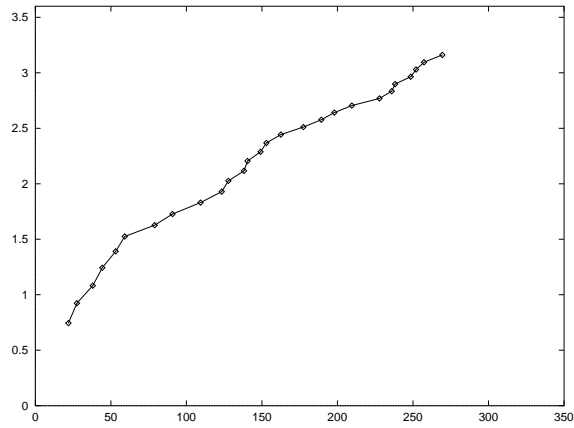


Figure 20. The cumulative distributions of the data set in Figure 18.

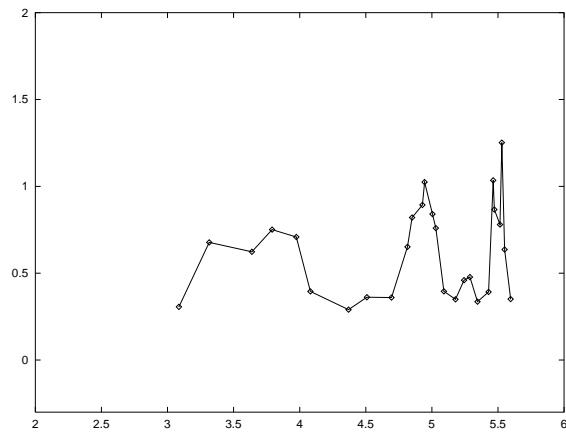


Figure 21. The logarithmic derivative of the cumulative distributions in Figure 20.

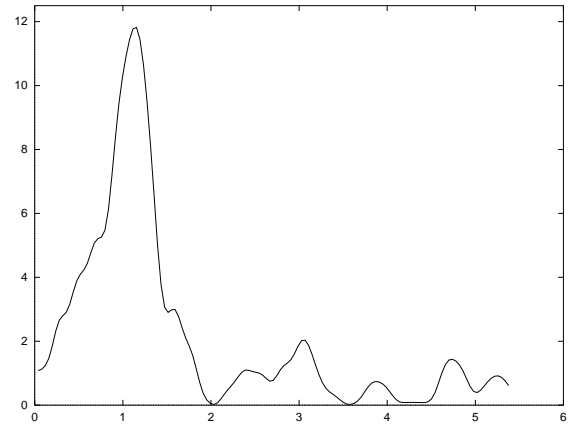


Figure 22. The Lomb periodogram of the derivative in Figure 19 at $f = 7/2\pi \approx 1.1$.

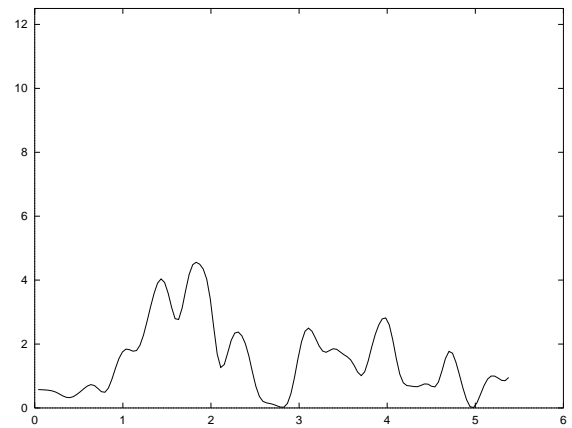


Figure 23. The Lomb periodogram of the derivative in Figure 21.

t :

$$\frac{d \ln N(t)}{d \ln t} = -p(t) ,$$

which defines the local (*i.e.*, at time t) Omori's exponent $p(t)$.

The maximum likelihood method is nonparametric and gives the most probable value of p given the data. In practice, we perform the maximum likelihood determination in a moving window from t to t_U . Moving t and t_U over the time axis allows us to capture local fluctuations in the Omori's p and provides us with a method whereby we can directly estimate any log-periodic oscillations [Lee, 1999].

3.1. Maximum Likelihood Estimation of Omori's Exponent

The maximum likelihood method estimates the p value in the window from t to t_U by maximizing the probability that the particular temporal distribution of the N events in that window results from Omori's law with this particular p value. The most likely p value is then given by the implicit equation

$$\frac{1}{p-1} + \frac{t_U^{p-1} \ln t - t^{p-1} \ln t_U}{t_U^{p-1} - t^{p-1}} = \langle \ln t \rangle_N , \quad (20)$$

where the t_n are the time occurrences of the N events between t and t_U and

$$\langle \ln t \rangle_N \equiv \frac{1}{N} \sum_{n=1}^N \ln t_n . \quad (21)$$

An expansion in powers of $(p-1) \ln t_U/t$ gives the explicit solution

$$p \approx 12 \frac{\ln \sqrt{t t_U} - \langle \ln t \rangle_N}{\left(\ln \frac{t_U}{t}\right)^2 + 1} , \quad (22)$$

with a typical error

$$\sigma \approx \sqrt{\frac{12}{(N-1) \left(\ln \frac{t_U}{t}\right)^2}} , \quad (23)$$

obtained from the negative Hessian of the log likelihood. Only the exponent p is estimated from the formulas. Expression (22) gives an extremely good approximation to the exact solution of Eq. (20), since the first nonzero correction is proportional to the fourth power $\approx 10^{-2} [(p-1) \ln t_U/t]^4$ of the expansion parameter. We have verified that the values p given by (22) are indistinguishable from the exact solution of (20) for the

range of p values of interest for aftershocks. Since the error σ is inversely proportional to the inverse of the square of the number N of events in the time window, probing smaller timescales is bought at a price of larger errors.

3.2. Generation of Log-Periodicity

Since the precision on the determination of p is essentially controlled by the number N of points in the running window, it seems natural to vary t_U as a function of t such that the number N of points in the running window remains fixed. Any other specification deteriorates the homogeneity of the determination of the exponent along the time axis. However, this procedure turns out to generate strong spurious log-periodicity as well. This is illustrated in Figure 24 showing the local p value in a running window with $N = 100$ events determined from a synthetic aftershock series generated using (16). The spectral analysis of this data set shown in Figure 25, confirms the statistical significance of the log-periodic signal.

By construction, the synthetic aftershock sequence obeys exactly Omori's law with $p = 1$, and any observed structure decorating this simple power law reflects random noise and finite size effects. We trace back the log-periodicity observed in Figure 24 to the constraint that the number of points N in the analyzing window is fixed. Indeed, for Omori's law with $p = 1$, this corresponds exactly to a sampling that is uniform in log time. As for the cumulative method, the most probable component of the noise has a significant spectral power.

3.2.1. Log frequency as a function of window size. To demonstrate the origin of log-periodicity in the maximum likelihood method with a fixed number of points in the running window, we generate 1000 synthetic aftershock series with 570 events and $p = 1.282$, corresponding to the values observed for the aftershock sequence of Long Beach 1933 documented by *Kisslinger and Jones* [1991]. For each of the 1000 synthetic sequences we have determined $p(t)$ in running windows of size $N = 12, 25, 50$, and 100 events. For a fixed window size N we took the Lomb periodogram of each $p(t)$ and then averaged them over the 1000 realizations. We thus obtain averaged Lomb periodograms for the four different values $N = 12, 25, 50$, and 100, shown in the Figures 26 and 27. It is clear that the dominating log frequency is a function of window size N .

The approximate lognormal shape of the Lomb periodograms shown in Figure 27 is remarkably consistent across the different values of the window size and is

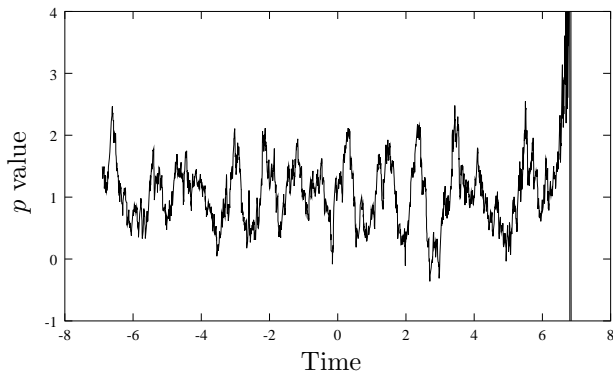


Figure 24. Omori's exponent p as a function of the logarithm of time in a running window of $N = 100$ events for a synthetic aftershock time series generated using (16) with $p = 1.0$, extending from time 1 to 1000 and containing ~ 500 events. Log-periodicity is clearly evident to the naked eye.

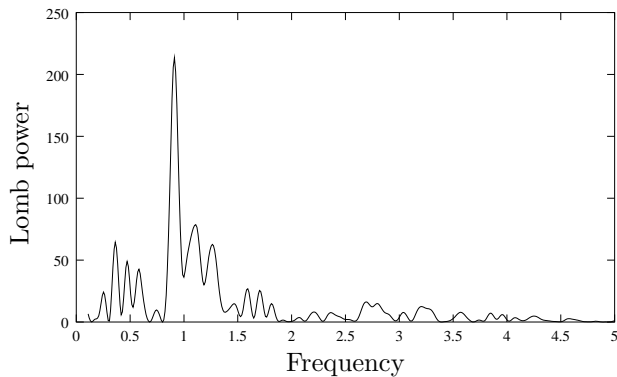


Figure 25. Lomb periodogram of Omori's exponent p shown in Figure 24 exhibiting a highly significant peak.

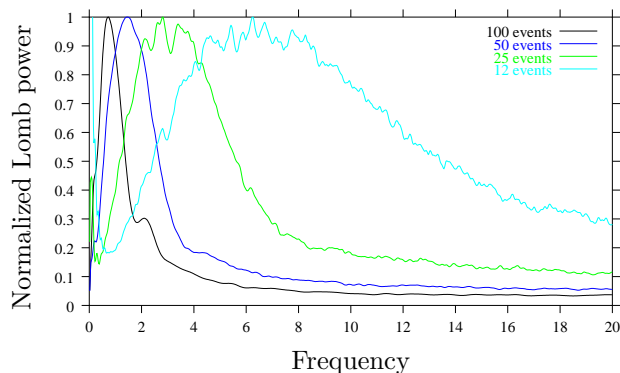


Figure 26. Average Lomb periodogram over 1000 synthetic aftershock realizations with 570 events and $p = 1.282$ of the function $p(t)$ calculated with the maximum likelihood method in running windows of size $N = 12, 25, 50$, and 100 events, respectively.

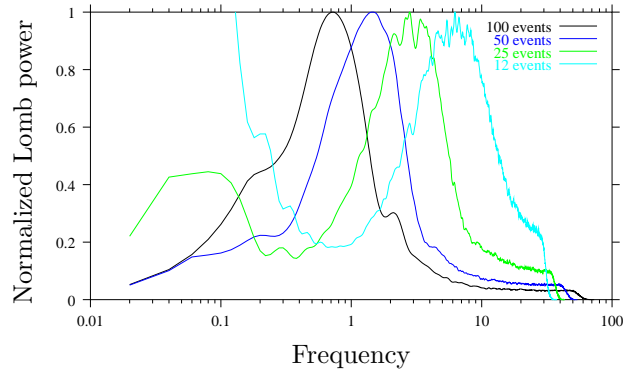


Figure 27. Same as Figure 26 using a log scale for the log frequencies illuminating the very similar approximate lognormal structure of the Lomb periodograms.

characterized by approximately the same standard deviation found close to 0.45 for all cases. A plot of the logarithm of the log frequency versus the logarithm of the window size N is given in Figure 28 showing that the log frequency is inversely proportional to N . For a point process with Omori's exponent close to 1, keeping a constant window size N is approximately equivalent to having windows with a constant value of t_U/t where t_U and t are the upper and lower times of the window:

$$f \sim \frac{1}{N} \quad (24)$$

$$\simeq \left(\ln \frac{t_U}{t} \right)^{-1}, \quad (25)$$

where N is window size. This reveals that using a fixed number of observations in each window corresponds to log sampling, a mechanism already identified as a source of log-periodicity.

Of course, for a single realization, fluctuations scramble the clear-cut result (24). This is illustrated in Figure 29 which tests the dependence of the most probable log frequencies of the $p(t)$ function as a function of window size N varying from 10 to 500. Figure 29 plots the most probable log frequency as a function of window size N for three cases. The first one corresponds to a synthetic sequence of 2000 events with exponent $p = 1.0$. The second one is for a real aftershock sequence, the North Palm Springs sequence of 1986, which contains 1437 events with $p \approx 1.14$. The last example is a numerical simulation of 2000 events from the $p = 1$ stress corrosion model of aftershocks studied [Lee and Sornette, 2000] with conservation parameter $\gamma = 0.15$, stress corrosion exponent $\alpha = 15$, and stress drop parameter $\beta = 0.999$, for which log-periodicity decorating Omori's law is very strong and thus strikingly visible directly on the $p(t)$

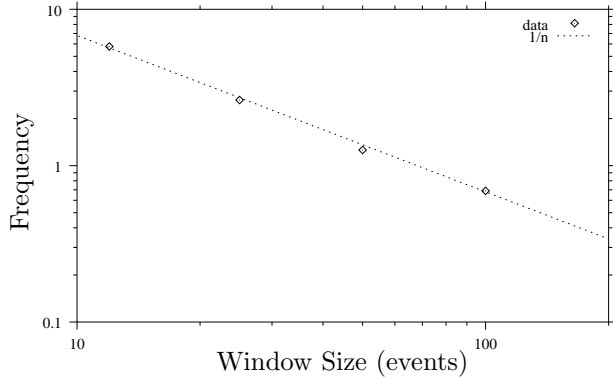


Figure 28. Dependence of the most probable log frequency (in logarithmic scale) corresponding to the maximum of the peaks in Figures 26 and 27 as a function of the logarithm of the window size N . The dashed line has a slope -1 .

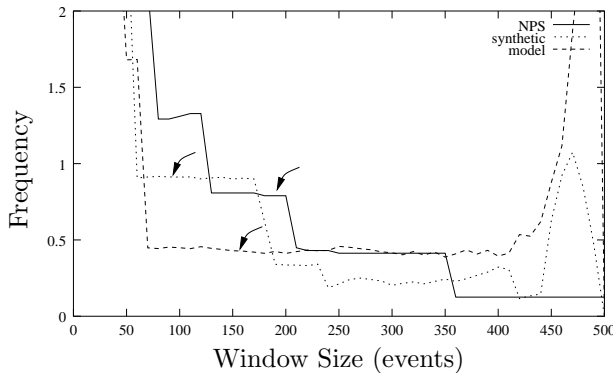


Figure 29. Log frequency as a function of window size N for a synthetic sequence, a real sequence (North Palm Springs of 1986 which contains 1437 events), and a sequence from the stress corrosion model studied by *Lee and Sornette* [2000].

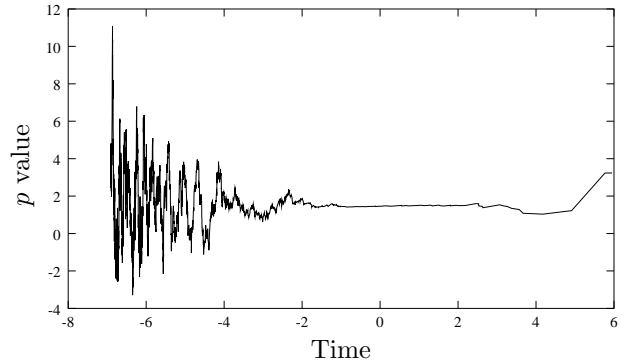


Figure 30. $p(t)$ as a function of the logarithm of time for a synthetic sequence generated with $p = 1.5$, 2000 events.

function (not shown). At large window sizes, multiple periods of log oscillation are included within a window, and Omori's exponent p starts to average out giving a very low value for the log frequency. At very small windows, small-scale variations dominate yielding anomalously high log frequencies. The optimal window sizes are small enough to cover less than a whole period of oscillation in order to resolve the oscillations but large enough not to be dominated by the small-scale variations. For the numerical simulation of the stress corrosion model of aftershocks studied by *Lee and Sornette* [2000], we observe a well-defined plateau for the log frequency as a function of window size N , extending from $N = 60$ to above 400, qualifying a genuine log-periodicity: the theoretical value of the log frequency is 0.41, [*Lee and Sornette*, 2000], which is consistent with the measured values. In contrast, the log frequency dependences of the synthetic Omori's law and of the North Palm Springs sequence are very similar to each other and show an overall decay as predicted by (24), decorated by fluctuations.

3.2.2. Log frequencies as a function of Omori's exponent p . Varying the value of Omori's exponent p away from 1 yields quantitatively different results. The functions $p(t)$ measured from synthetic time series generated with $p = 1.5$ and $p = 0.5$ are given in Figures 30 and 31. Three features can be observed: (1) the log frequency has increased in both cases; (2) the oscillations are no longer truly log-periodic since the log frequency decreases with time for $p = 1.5$ and increases with time for $p = 0.5$; and (3) the amplitude of oscillations changes with time in both cases. To recover regular oscillations, we see from (16) that one would need to plot $p(t)$ as a function of t^{1-p} instead of $\ln t$, which is the correct variable only for series with constant $p = 1$.

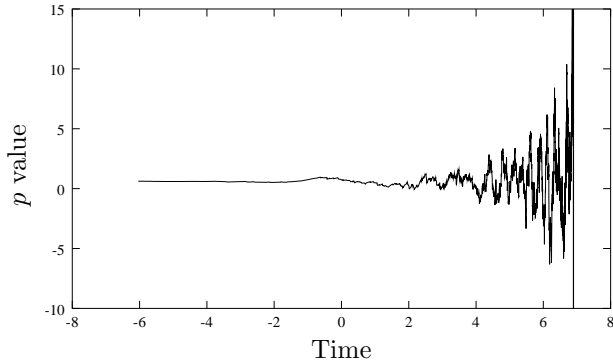


Figure 31. $p(t)$ as a function of the logarithm of time for a synthetic sequence generated with $p = 0.5$, 2000 events.

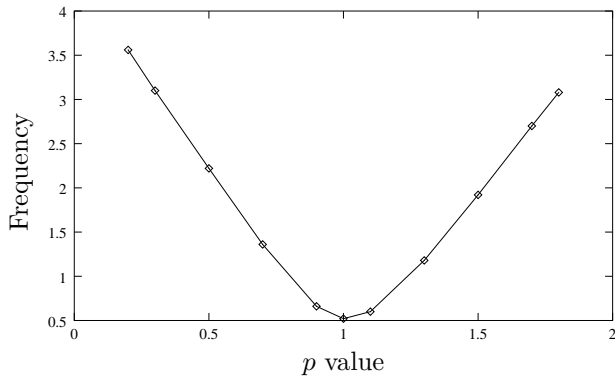


Figure 32. Average log frequency as a function of p value for synthetic aftershock sequences.

Notwithstanding its variation with time, we determine the log frequency of the dominant peak by averaging over the Lomb periodograms of 100 realizations of synthetic data. The dependence of the average log frequency as a function of the exponent p used in generating synthetic aftershock sequences is presented in Figure 32. For each p value the average frequency has been averaged over 100 realizations. As p differs from 1, the sequence exhibits higher and higher log frequencies. Figure 32 recovers the results already shown in Figure 8 for the cumulative method.

We have attempted to use the insight provided by Figures 28, 29, and 32 to distinguish the log-periodic signatures observed in real aftershock sequences from those obtained in synthetic data sets with the maximum likelihood approach. We estimate the log frequency in the real aftershock sequences as shown by the arrows in Figure 29 on a plateau in a central region for the window size which seems to provide a reasonable compromise as explained above. Each of the real aftershock

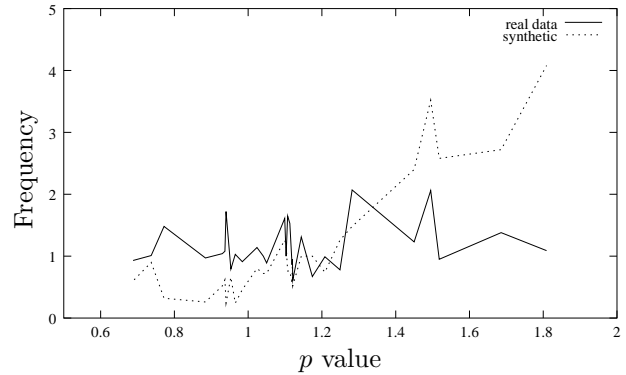


Figure 33. Average log frequency as a function of Omori's exponent p in real and synthetic sequences. The confidence bounds are seen from the size of the fluctuations of the synthetic data.

sequences is characterized by its average p value determined by *Kisslinger and Jones* [1991]. We use this p value to generate 1000 synthetic sequences with the same number of events. We record the log frequency of the largest peak of the Lomb periodogram of the function $p(t)$ for each of these 1000 synthetic sequences and then average it. Spanning the different real aftershock sequences allows us to span a relatively large interval of p values. We thus represent in Figure 33 the most probable log frequency as a function of average p value obtained from the set of real aftershock sequences and their corresponding synthetic ensemble. As in Figure 32, the synthetic log frequency average is increasing for $p > 1$ (notwithstanding the averaging over 1000 realizations, fluctuations remain apparent). In contrast, the most probable log frequency obtained for the real aftershock sequences do not seem to be noticeably dependent on the average p . This difference suggests that log-periodicity in real aftershock sequences could be real. However, the difference is weak and not clearly above noise level. By itself, this result is suggestive but not enough to substantiate the claim of log-periodicity in real data [*Lee and Sornette*, 2000].

3.3. Can Log-Periodicity Be “Saved” for Aftershocks?

3.3.1. Fixed time window size. In view of the spurious log-periodicity generated when using a constant number of points in a moving window which is equivalent to log sampling, we redo all calculations using the maximum likelihood approach with windows of fixed duration (for instance one-day windows). These calculations are performed on all sequences documented

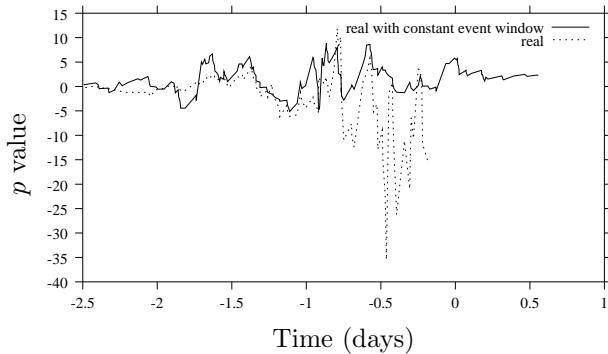


Figure 34. Comparison of the local $p(t)$ as a function of the logarithm of time for event 29 (Westmoreland aftershock sequence) in the list of *Kisslinger and Jones* [1991] using the maximum likelihood method with a running window of fixed time duration of 0.1 day and with a fixed number of aftershocks (log sampling). We observe structures that are common to the two methods: this may be the signature of a real log-periodicity.

by [*Kisslinger and Jones*, 1991] as well as on the more recent Loma Prieta, Landers, and Northridge aftershock sequences. As typical examples, we show the 1981 Westmoreland and 1989 Loma Prieta aftershock sequences. We choose the Westmoreland as an example with $p > 1.4$ and also with fluctuations greater than one standard deviation (2σ) from the mean equal to one (Figure 34). Loma Prieta is chosen as an example of a more recent sequence with a more complete record. It also exhibits fluctuations in the local $p(t)$ greater than 2σ . Using a running time window which is fixed to 0.1 days, the Omori's exponent p for the Westmoreland and for Loma Prieta aftershock sequences appear to fluctuate log-periodically with a log frequency around 1. The solid lines are for a constant number of events in the running window, while the dashed lines are for fixed time windows. In the two examples shown here and for a majority of the real aftershock sequences studied here, peaks are found at log frequencies near 1 (see the peaks in solid and dashed lines close to the abscissa 1 in Figure 35).

Table 3 lists the top three local peak maxima in frequency with their associated spectral power from the Lomb periodogram for all analyzable real aftershock sequences, using the maximum likelihood method with fixed time window. The sequence numbers are as given by *Kisslinger and Jones* [1991]. The amplitude of the fluctuations in p values in running time windows as a function of time is given in integer units of the standard deviation around the average calculated for each

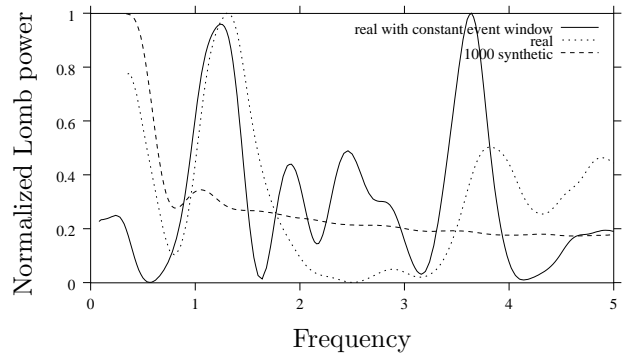


Figure 35. Comparison of the Lomb periodograms corresponding to the two signals shown in Figure 34. We observe a common peak at a log frequency close to 1.2.

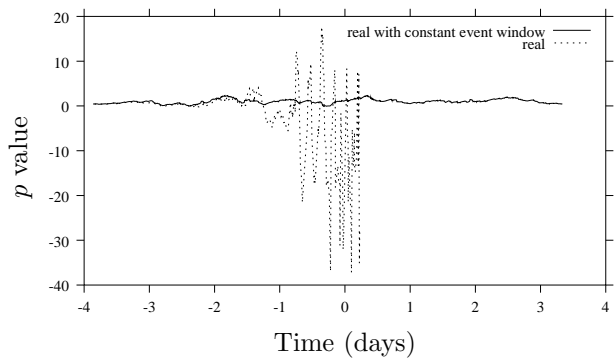


Figure 36. Same as Figure 34 for the Loma Prieta aftershock sequence.

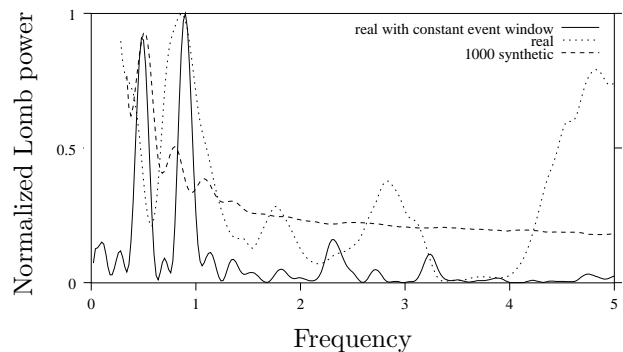


Figure 37. Same as Figure 35 for the Loma Prieta aftershock sequence. We also observe a common peak at a log frequency close to 1 and a slightly smaller one at approximately half log frequency.

Table 3. List of the Top Three Local Peak Maxima in Frequency With Their Associated Spectral Power From the Lomb Periodogram for All Analyzable Real Aftershock Sequences, Using the Maximum Likelihood Method With Fixed Time Window^a

Sequence	Amplitude(σ)	window (days)	f_1	f_2	f_3	$power_1$	$power_2$	$power_3$
1	2	150	4.18	3.61	2.60	13.74	11.84	8.42
5	1	1	0.71	1.18	1.65	4.68	2.52	2.14
6		1	1.61	1.80	1.38	2.65	2.58	2.26
7	1	100	1.90	0.79	1.57	5.67	5.16	5.11
8	1	10	0.56	1.48	4.20	5.85	3.42	3.34
9	1	1	4.01	4.95	1.50	2.83	2.63	2.61
10		1	1.79	1.47	4.20	3.13	2.16	1.75
11		1	2.35	2.63	0.76	2.00	1.69	1.53
12		1	0.63	3.14	1.84	4.27	2.23	1.48
13	1	1	1.48	1.55	2.48	3.01	2.95	2.24
14	2	100	1.59	3.65	2.06	16.73	13.43	5.49
15		1	0.63	0.89	2.99	3.37	2.64	2.54
18		1	0.52	4.39	2.87	4.57	3.82	3.78
19		10	0.66	1.33	2.78	3.92	1.38	1.31
20		1	0.96	2.82	2.91	3.91	2.94	2.86
21		10	0.61	1.22	0.84	2.18	2.11	1.60
22	1	1	2.47	2.30	0.69	4.79	4.69	4.64
23		1	1.19	0.69	1.88	4.70	1.38	1.17
24	1	1	1.31	1.07	1.45	4.96	3.99	3.66
25	1	1	2.53	2.22	1.99	6.49	4.97	4.06
26	1	1	0.70	4.13	3.03	22.82	18.04	11.46
27		1	0.76	4.34	0.56	2.56	2.16	2.01
28	2	1	1.25	1.47	2.36	7.45	7.07	5.86
29	1	0.1	1.30	3.84	4.87	13.07	6.57	6.08
30		1	0.66	3.55	0.96	5.61	4.69	3.07
31	2	1	4.06	3.45	1.72	15.44	5.87	5.37
32		1	0.53	1.38	1.68	6.62	5.12	4.87
33	1	1	1.41	3.57	2.70	30.14	23.42	16.79
34	2	10	0.58	3.77	1.50	19.68	15.43	7.41
35		1	0.55	4.85	1.65	3.94	3.08	2.31
36		1	1.42	1.65	2.22	8.89	8.42	7.70
Loma Prieta	2	0.1	0.86	4.83	4.55	15.91	12.59	9.53
Landers	2	1	4.06	4.85	0.97	19.14	17.11	16.09
Northridge	2	10	0.60	1.04	4.20	50.54	49.38	19.36

^aThe sequence numbers are as *Kisslinger and Jones* [1991]. The amplitude of the fluctuations in p values in running time windows as a function of time is given in integer units of the standard deviation around the average calculated for each sequence.

^aThe sequence numbers are as *Kisslinger and Jones* [1991]. The amplitude of the fluctuations in p values in running time windows as a function of time is given in integer units of the standard deviation around the average calculated for each sequence.

sequence.

3.3.2. Lomb averaging. The case for log-periodicity in earthquake aftershocks is quite weak. We have shown that the maximum likelihood method with running windows of a fixed number of events generates spurious log-periodicity with a log frequency inversely proportional to the window size. Furthermore, the measured frequencies do not significantly deviate from those found from 1000 synthetic sequences. We moved to the maximum likelihood method with a fixed time window to remove the log sampling effect. The results were slightly more encouraging. We have also tried to analyze fluctuations of the difference between the cumulative number of aftershocks and its smoothed Omori’s law. Although the structures generated by this method were in good agreement with the p value structure from the maximum likelihood method, the fact that both methods give similarly correlated structures on synthetic data does not enhance the evidence.

We now turn to a last investigation using averaging. As shown by *Johansen et al.* [2000b], averaging over Lomb periodograms provides in principle a powerful method to retrieve the presence of log-periodicity if the log frequencies are similar from sequence to sequence. This is due to the fact that the Lomb periodograms are not sensitive to the phase of the log-periodic oscillations, and we do not run the risk of scrambling the log-periodic oscillations due to their random phases, as would occur during a direct averaging of the $p(t)$ functions for instance. See also *Johansen and Sornette* [1998] for a general discussion of the caveats of ensemble averaging.

Figure 38 shows the average Lomb periodogram obtained by using all real aftershock sequences. It should be compared to Figure 39 obtained by averaging the Lomb periodograms of 1000 synthetic realizations for each real aftershock sequence. We see that the peak is differently positioned for the real aftershock sequences compared to that of the synthetic.

Encouraged by this, we have singled out all real aftershock sequences where the fluctuations around the average Omori’s law of $p = 1$ was greater than 1 and 2σ . The result is shown in Figures 40 and 41. We see that a stronger log-periodic signal appears in the spectra of the real aftershock sequences compared to that of the synthetic. By this, we observe that the peak culminating at 1 of the solid line (real data) is significantly sharper than that for the synthetic ensemble. This indicates that genuine log-periodic structures might be more easily identified in sequences with “anomalous” high or low p value and large fluctuations.

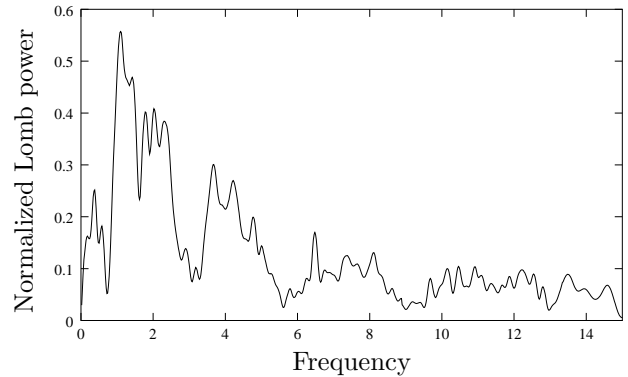


Figure 38. Average Lomb periodogram over all real aftershock sequences using the maximum likelihood method with running windows of a constant number of events (log sampling).

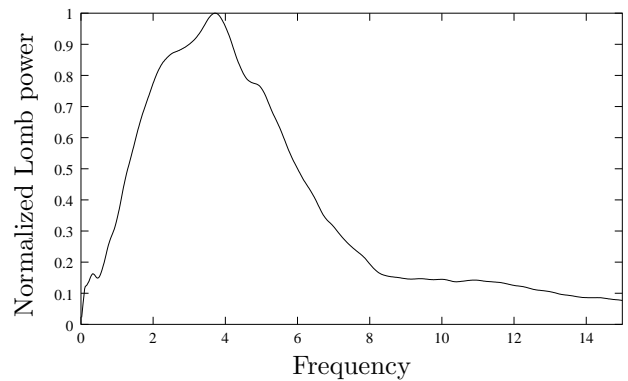


Figure 39. Same as Figure 38 but for 1000 synthetic sequences for each real aftershock sequence with the same parameters.

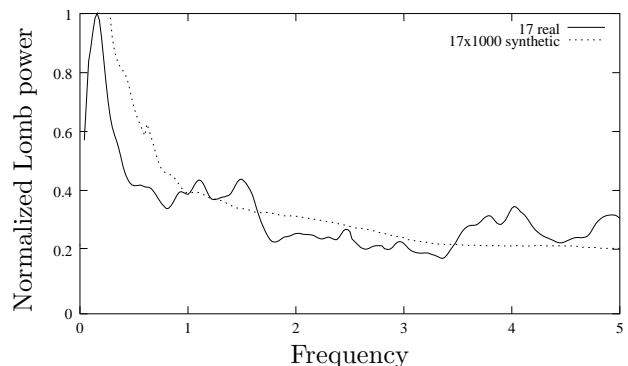


Figure 40. The solid line is the average Lomb periodogram over the subset of 17 real aftershock sequences for which the p value fluctuations are greater than 1σ . The dashed line is the average over 17,000 synthetic aftershock sequences, 1000 for each of the 17 real ones with p value fluctuations greater than 1σ .

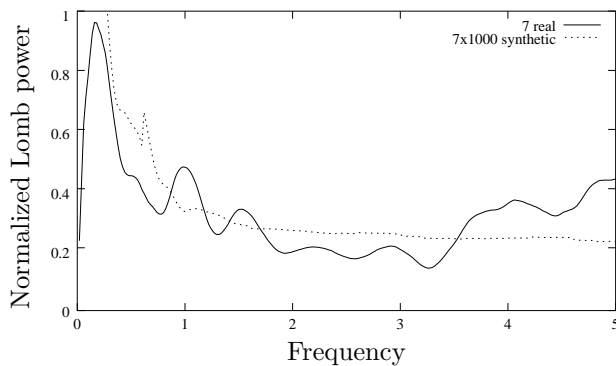


Figure 41. The solid line is the average Lomb periodogram over the subset of seven real aftershock sequences for which the p value fluctuations are greater than 2σ . The dashed line is the average over 7000 synthetic aftershock sequences, 1000 for each of the seven real ones with p value fluctuations greater than 2σ .

4. Discussion

We have presented a detailed study of log-periodicity in relatively sparse data with nonuniform sampling. We have focused our attention on the effect of this nonuniform sampling and its interplay with integration in the presence of noise, which may lead to synthetically generated log-periodicity that may compete with genuine signals. Our main result is the discovery that approximately logarithmic sampling and integration (performed either by constructing cumulative functions or using a maximum likelihood method) generate strong log-periodic structures. This result calls for a reassessment of previous reports of log-periodicity in rupture [Anifrani *et al.*, 1995; Sahimi and Arbabi, 1996; Huang *et al.*, 1997; Johansen and Sornette, 1998] and in earthquakes [Sornette and Sammis, 1995; Saleur and Sornette, 1996; Saleur *et al.*, 1996a, b; Johansen *et al.*, 1996; Varnes and Bufe, 1996; Lee, 1999] in the spirit of the reanalysis [Johansen *et al.*, 2000a] of the evidence for criticality and especially log-periodicity in the previously reported chemical anomalies that preceded the Kobe earthquake. In this recent work [Johansen *et al.*, 2000a], the ion (Cl^- , K^+ , Mg^{++} , NO_3^- and SO_4^{--}) concentrations of groundwater issued from deep wells located near the epicenter of the 1995 Kobe earthquake are taken as proxies for the cumulative damage preceding the earthquake. Using both a parametric and nonparametric analysis following the guidelines given in this paper, the five data sets are compared extensively to synthetic time series. The null hypothesis that the patterns documented on these times series result from

noise decorating a simple power law is rejected with a very high confidence level. For the other cases of reported log-periodicity, we plan to present a reanalysis in forthcoming publications.

We have also analyzed in detail the 27 best aftershock sequences studied by Kisslinger and Jones [1991] and the Loma Prieta, Landers, and Northridge aftershock sequences for the presence of log-periodic corrections to Omori’s law. Both the cumulative distribution and maximum likelihood methods lead to synthetic log-periodicity resulting from the interplay between noise reddening and power law scaling. However, it is important to distinguish between the two processes. The low-pass filtering resulting from the integration used to generate the cumulative distribution is very different from the averaging process used in the maximum likelihood method. In the latter, the upper frequency cutoff is completely determined by the data window used in the estimation process. Most of the structures observed on the 27 aftershock sequences can be explained solely on the basis of the spurious log-periodicity generated by the nonuniform sampling and the integration mechanism. There are some residual structures in aftershock sequences of possible log-periodic origin which cannot be fully explained by the synthetic scenario. Hence the possibility of a signal resulting from a physically based log-periodicity as claimed by Lee [1999] cannot be ruled out. Better quality data with an order of magnitude more events are needed to resolve this issue.

A tantalizing question is whether the spurious log-periodic oscillations that might appear in the analysis of a foreshock sequence can still be used to improve the prediction of the main event. This would be equivalent to “fitting the most probable form of noise,” an attractive though maybe not workable idea. We hope to report on this point soon.

Acknowledgments. We are grateful to C. Kisslinger for sharing his data with us.

References

- Anifrani, J.-C., C. L. Floc’h, D. Sornette, and B. Souillard, Universal log-periodic correction to renormalization-group scaling for rupture stress prediction from acoustic emissions, *J. Phys. I*, 5, 631–638, 1995.
- Barton, C., and P. L. Pointe (Eds.), *Fractals in Petroleum Geology and Earth Processes*, Plenum, New York, 1995.
- Bowman, D., G. Ouillon, C. Sammis, A. Sornette, and D. Sornette, An observational test of the critical earthquake concept, *J. Geophys. Res.*, 103, 24,359–72, 1998.
- Brehm, D., and L. Braile, Intermediate-term earthquake prediction using the modified time-to-failure method in

- Southern California, *Bull. Seism. Soc. Am.*, *89*, 275–93, 1999.
- Geller, R., D. Jackson, Y. Kagan, and F. Mulargia, Geoscience–Earthquakes cannot be predicted, *Science*, *275*, 1616–7, 1997.
- Gross, S., and J. Rundle, A systematic test of time-to-failure analysis, *Geophys. J. Int.*, *133*, 57–64, 1998.
- Huang, Y., G. Ouillon, H. Saleur, and D. Sornette, Spontaneous generation of discrete scale invariance in growth models, *Phys. Rev. E*, *55*, 6433–6447, 1997.
- Johansen, A., and D. Sornette, Evidence of discrete scale-invariance in DLA and time-to-failure by canonical averaging, *Int. J. Modern Phys. C*, *9*, 433–447, 1998.
- Johansen, A., D. Sornette, H. Wakita, U. Tsunogai, W. Newman, and H. Saleur, Discrete scaling in earthquake precursory phenomena: Evidence in the Kobe earthquake, Japan, *J. Phys. I*, *6*, 1391–1402, 1996.
- Johansen, A., H. Saleur, and D. Sornette, New evidence of earthquake precursory phenomena in the 17 January 1995 Kobe earthquake, Japan, *Euro. Phys. J. B*, *15*, 551–5, 2000a.
- Johansen, A., D. Sornette, and A. Hansen, Punctuated vortex coalescence and discrete scale invariance in two-dimensional turbulence, *Physica D*, *138*, 302–15, 2000b.
- Kisslinger, C., and L. Jones, Properties of aftershock sequences in southern California, *J. Geophys. Res.*, *96*, 11,947–58, 1991.
- Lee, M., Unstable fault interactions and the self-organization of earthquake aftershocks, Ph.D. thesis, University of California, Los Angeles, 1999.
- Lee, M., and D. Sornette, Novel mechanism for discrete scale invariance in sandpile models, *Euro. Phys. J. B*, *15*, 193–7, 2000.
- Newman, W., D. Turcotte, and A. Garielov, Log-periodic behavior of a hierarchical failure model with applications to precursory seismic activation, *Phys. Rev. E*, *42*, 4827, 1995.
- Onsager, L., *Phys. Rev.*, *65*, 117, 1944.
- Ouillon, G., and D. Sornette, The critical earthquake concept applied to mine rock bursts with time-to-failure analysis, in *The Earth, Earthquakes and Seismic Waves: The Knopoff Volume*, Geophys. J. Int. Monograph, 2000.
- Ouillon, G., D. Sornette, and C. Castaing, Organization of joints and faults from 1 cm to 100 km scales revealed by optimized anisotropic wavelet coefficient method and multi-fractal analysis, *Nonlinear Processes Geophys.*, *2*, 158–77, 1995.
- Ouillon, G., C. Castaing, and D. Sornette, Hierarchical scaling of faulting, *J. Geophys. Res.*, *101*, 5477–87, 1996.
- Press, W., S. Teukolsky, W. Vetterling, and B. Flannery, *Numerical Recipes in FORTRAN: The Art of Scientific Computing*, Cambridge Univ. Press, New York, 1992.
- Reasenber, P., Second-order moment of central California seismicity, 1969–1982, *J. Geophys. Res.*, *90*, 5479, 1985.
- Reasenber, P., Foreshock occurrence before large earthquake, *J. Geophys. Res.*, *104*, 4755–68, 1999.
- Sahimi, M., and S. Arbabi, Scaling laws for fracture of heterogeneous materials and rock, *Phys. Rev. Lett.*, *77*, 1689, 1996.
- Saleur, H., and D. Sornette, Complex exponents and log-periodic corrections in frustrated systems, *J. Phys. I*, *6*, 327–355, 1996.
- Saleur, H., C. Sammis, and D. Sornette, Renormalization group theory of earthquakes, *Nonlinear Processes Geophys.*, *3*, 102, 1996a.
- Saleur, H., C. Sammis, and D. Sornette, Discrete scale invariance, complex fractal dimensions, and log-periodic fluctuations in seismicity, *J. Geophys. Res.*, *101*, 17,661–17,677, 1996b.
- Scholz, C., and B. Mandelbrot (Eds.), *Fractals in Geophysics*, Birkhauser, Cambridge, Mass., 1989.
- Slutzky, E., The summation of random causes as the source of cyclic processes, *Econometrica*, pp. 105–46, 1937.
- Sornette, D., Discrete scale invariance and complex dimensions, *Physics Reports*, *297*, 239–270, 1998.
- Sornette, D., Log-periodic time-to-failure analysis, in *Proceedings of SPIE Conference on NDE of Ageing Aircraft, Airports and Aerospace Hardware*, edited by A. Mal, p. 178, SPIE int. Soc. for Opt. Eng., Bellingham, Wash., 1999.
- Sornette, D., *Critical Phenomena in Natural Sciences, Chaos, Fractals, Self-organization and Disorder: Concepts and Tools*, Springer Series in Synergetics, Springer, Heidelberg, 2000.
- Sornette, D., and C. Sammis, Complex critical exponents from renormalization group theory of earthquakes: implications for earthquake predictions, *J. Phys. I*, pp. 607–619, 1995.
- Sornette, D., A. J. A. Arneodo, J.-F. Muzy, and H. Saleur, Complex fractal dimensions describe the hierarchical structure of diffusion-limited-aggregate clusters, *Phys. Rev. Lett.*, *76*, 251–254, 1996.
- Stratonovich, R., *Topics in the Theory of Random Noise*, vol. I and II, Gordon and Breach, New York, 1967.
- Tsunogai, U., and H. Wakita, Precursory chemical changes in ground water–Kobe earthquake, Japan, *Science*, *269*, 61–63, 1995.
- Tsunogai, U., and H. Wakita, Anomalous changes in ground water chemistry–Possible precursors of the 1996 Hyogoken Nanbu earthquake, Japan, *J. Phys. Earth*, *44*, 381–90, 1996.
- Turcotte, D., *Fractals and Chaos in Geology and Geophysics*, 2nd ed., Cambridge Univ. Press, New York, 1997.
- Utsu, T., Y. Ogata, and R. Matsu’ura, The centenary of the Omori formula for a decay law of aftershock activity, *J. Phys. Earth*, *43*, 1–33, 1995.
- Varnes, D., and C. Bufe, The cyclic and fractal seismic series preceding an M(b) 4.8 earthquake on 1980 February 14 near the Virgin-Islands, *Geophys. J. Int.*, *124*, 149–158, 1996.
- Zajdenweber, D., *Hasard et Prevision*, Economica, Paris, 1976.

Y. Huang and H. Saleur, Department of Physics, University of Southern California, Los Angeles, CA 90089-0484. (e-mail: yueqiang@usc.edu; saleur@usc.edu)

A. Johansen and M. W. Lee, Institute of Geophysics and Planetary Physics, University of California, 3845 Schlichter Hall, Los Angeles, CA 90095-1567. (e-mail: anders@moho.ess.ucla.edu; lee@physics.ucla.edu)

D. Sornette, Laboratoire de Physique de la Matière Condensée, CNRS UMR 6622 and Université de Nice-

Sophia Antipolis, B.P. 70, Parc Valrose, F-06108 Nice Cedex 2, France.. (e-mail: Didier.Sornette@unice.fr)

Received October 28, 1999; revised March 9, 2000; accepted May 30, 2000.

This preprint was prepared with AGU's L^AT_EX macros v5.01, with the extension package 'AGU++' by P. W. Daly, version 1.6b from 1999/08/19.